SERI/STR-211-2813
(DE85016880)

RESEARCH ON HIGH-EFFICIENCY, SINGLE-JUNCTION, MONOLITHIC, THIN-FILM a-Si SOLAR CELLS

Annual Subcontract Progress Report for the Period
February 1, 1984—January 31, 1985

By
D. E. Carlson
A. Catalano
R. V. D'Aiello
C. R. Dickson
R. S. Oswald

November 1985

Work Performed Under Contract No. AC02-83CH10093

Solarex Thin Film Division
Newtown, Pennsylvania

and

Solar Energy Research Institute
Golden, Colorado

Technical Information Center
Office of Scientific and Technical Information
United States Department of Energy

DISCLAIMER

Available from the National Technical Information Service, U. S. Department of Commerce, Springfield, Virginia 22161.

Price: Printed Copy A05
Microfiche A01

Codes are used for pricing all publications. The code is determined by the number of pages in the publication. Information pertaining to the pricing codes can be found in the current issues of the following publications, which are generally available in most libraries: *Energy Research Abstracts (ERA); Government Reports Announcements* and Index *(GRA* and I); *Scientific and Technical Abstract Reports (STAR);* and publication NTIS-PR-360 available from NTIS at the above address.

Printed in the United States of America
USDOE Office of Scientific and Technical Information
Oak Ridge, Tennessee

SERI/STR-211-2813
(DE85016880)
Distribution Category UC-63

Research on High-Efficiency, Single-Junction, Monolithic, Thin-Film a-Si Solar Cells

Annual Subcontract Progress Report
1 February 1984 - 31 January 1985

D. E. Carlson
A. Catalano
R. V. D'Aiello
C. R. Dickson
R. S Oswald

Solarex Thin Film Division
Newtown, Pennsylvania

November 1985

Prepared under Subcontract No. ZB-4-03056-3
SERI Technical Monitor: W. Wallace

Solar Energy Research Institute
A Division of Midwest Research Institute

1617 Cole Boulevard
Golden, Colorado 80401

Prepared for the
U.S. Department of Energy
Contract No. DE-AC02-83CH10093

SUMMARY

Task No. 1: Amorphous Silicon Materials Research

Five glow discharge deposition systems including an in-line, multi-chamber system have been set up and are being used to grow both doped and undoped a-Si:H material. Analyses of silane cylinders with gas chromatography/mass spectroscopy reveals that disiloxane is a deleterious contaminant found in some cylinders. Contaminants such as n-butane and ethyl silane were detected in disilane gas cylinders. Compositional analyses of a-Si:H films show that the total impurity content is on the order of $10^{19}cm^{-3}$ with oxygen dominating. The diffusion lengths of undoped a-Si:H films are typically $\sim$ 0.3 - 0.4μm after 48 hours of AM1 illumination. Preliminary results indicate that light-induced effects are minimized by means of slow deposition rates.

Task No. 2: Non-Semiconductor Materials Research

A laboratory CVD belt furnace has been used to make textured tin oxide-coated glass with a sheet resistivity of $\sim$ 20 $\Omega/\square$. Trial runs with a Watkins-Johnson CVD belt furnace have produced tin oxide films with a sheet resistivity of 10 $\Omega/\square$ and absorption losses of $\sim$ 10%. Metal back contacts such as Al, Ni, Ti, and Mg are being deposited on the n layers of p-i-n solar cells by means of either an S-gun metallization system, an electron beam evaporation system or an in-line sputter deposition system. EVA/Tedlar films have been laminated to the back of a-Si:H solar-cell modules, and no adverse effects have been observed to date after repeated temperature-humidity cycles.

Task No. 3: Solar-Cell Research

A conversion efficiency of 10.5% has been obtained for a p-i-n cell with an area of $0.051cm^2$; 10.3% was achieved with devices of $0.2cm^2$. The cell configuration is glass/SnO_2/p^*-i-n/Al where the p^* layer is p-type a-Si:C:H. The substrate for these devices consists of textured tin oxide on pyrex glass. Stability studies show less light-induced degradation for cells with thin i-layers and for cells operating at elevated temperatures.

Task No. 4: Monolithic, Intra-Connected Cells/Submodule Research

A baseline submodule has been designed with 12 parallel strings each containing 35 series-connected cells on a 12" x 13" substrate. A conversion efficiency of 6.07% was obtained for a submodule with 9 active strings (active area = 630cm^2). An experimental laser scribing system with automatic focusing and multiple beam capability has been ordered for delivery in March 1985. An existing Solarex laser scribing system is being used to pattern both tin oxide and a-Si:H over areas up to 1000cm^2. Laser scribing has also been used to pattern the back metal contact over areas up to 400cm^2.

Task No. 5: Multi-Chamber Deposition System

A conceptual design was completed for a multi-chamber deposition system that incorporates features such as external heaters, heated rf electrodes and gas curtains for dopant isolation. A Solarex multi-chamber deposition system has demonstrated uniform depositions of a-Si:H over areas of 1000cm^2 and has produced submodules with efficiencies $\sim$ 6%.

TABLE OF CONTENTS

FIGURE CAPTIONS

LIST OF TABLES

ABSTRACT

This research program consisted of five tasks. Task 1, Amorphous Silicon Materials Research, involved producing and optimizing amorphous silicon material. Task 2, Non-Semiconductor Materials Research, involved producing nonsemiconductor materials required to make high-performance, amorphous silicon solar cells. Task 3, Solar Cell Research, involved fabricating and characterizing high-efficiency, single-junction, p-i-n amorphous silicon solar cells. In Task 4, Monolithic, Intra-Connected Cells/Submodule Research, research and development was performed to produce submodules of monolithic, intraconnected solar cells. In Task 5, Multi-Chamber Deposition System, a multi-chamber system was designed to fabricate submodules of at least 1000 cm^2. The major goals of the program are (1) to obtain a conversion efficiency of at least 12% (AM1) in a single-junction, p-i-n, 1-cm^2 solar cell; (2) to eliminate the deleterious effects of light-induced, metastable centers; (3) to operate a multi-chamber deposition a-Si growth system; and (4) to demonstrate a stable submodule with an 8% conversion efficiency (AM1) and a total area of at least 1000 cm^2.

SECTION 1.0

INTRODUCTION

This research program consists of five tasks. Task 1, Amorphous Silicon Materials Research, is directed toward producing and optimizing amorphous silicon material. Task 2, Non-Semiconductor Materials Research, involves the production and optimization of non-semiconductor materials that are required to make high performance, amorphous silicon solar cells. Task 3, Solar Cell Research, involves the fabrication and characterization of high efficiency, single-junction p-i-n amorphous silicon solar cells. In Task 4, Monolithic, Intra-Connected Cells/Submodule Research, we are performing the research and development necessary to produce submodules of monolithic, intra-connected solar cells. Task 5, Multi-Chamber Deposition System, involves the use of a multi-chamber system to fabricate submodules with an area of at least $1000cm^2$. This task has also involved the conceptual design of a multi-chamber deposition system as shown in Section 6.0 of this report.

The major goals for the three year program are: (1) to obtain a conversion efficiency of at least 12% (AM1) in a single-junction p-i-n solar cell with an area of at least $1cm^2$; (2) to eliminate the deleterious effects of light-induced, metastable centers so that cell efficiency does not change by more than 2% (relative) over at least 720 hours of continuous AM1 illumination; (3) to operate a multi-chamber deposition system for growing amorphous silicon material; and (4) to demonstrate a stable submodule with a conversion efficiency of at least 8% (AM1) and a total area of at least $1000cm^2$.

SECTION 2.0

TASK NO. 1: AMORPHOUS SILICON MATERIALS RESEARCH

2.1 INTRODUCTION

Because amorphous silicon solar cell efficiency is ultimately limited by material quality, amorphous silicon materials research is critical. Both doped and undoped amorphous silicon thin films for use in solar cells are being prepared by dc and rf glow discharge depositions. To optimize the materials for amorphous silicon solar cells, film purity is being monitored, electronic and optical measurements are being performed, and the effects of deposition rate on the film properties are being determined by varying deposition parameters. These films are also being evaluated under optical illumination to analyze the mechanism responsible for light-induced changes in the materials.

2.2 PREPARATION OF AMORPHOUS SILICON FILMS

To prepare both doped and undoped amorphous silicon films, four deposition systems are presently used. Two of these systems operate in the batch mode depositing films using a dc glow discharge. One of the systems has a load- lock and operates in either the dc or rf deposition mode. Another system at Vactronics operates in the rf glow discharge mode. Because the load lock system primarily will be used for amorphous silicon materials research, it will be described in detail below. All systems are computer controlled to ensure reliability during the deposition sequence. All four systems were operational ahead of schedule.

The load-lock deposition system (see Fig. 2.1) has many features which make it desirable to optimize amorphous silicon materials. The load lock allows substrates to enter the main deposition system without breaking vacuum. Consequently, it is similar to the multi-chamber deposition system. The load-lock permits many experiments to be performed daily, unlike most batch deposition systems. Up to 22 runs have been made without affecting the performance of fabricated solar cells. In addition, this system has fabricated solar cells on substrates with areas as large as 420 cm^2. This system can strike a glow discharge using either dc or rf power sources and the electrode distance can be varied from outside the main deposition chamber. The system

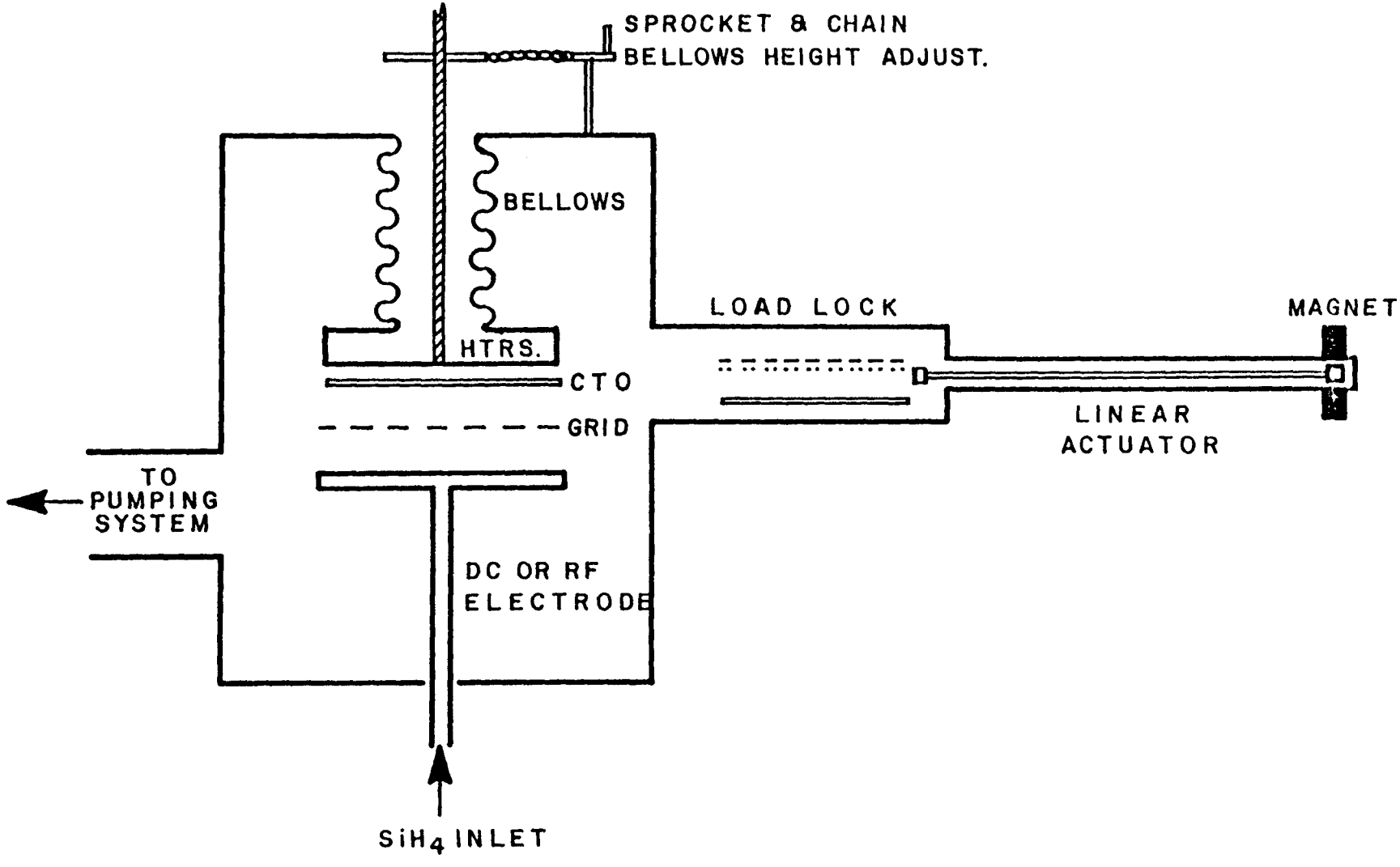

FIGURE 2-1. SCHEMATIC DIAGRAM OF THE SOLAREX SINGLE LOAD-LOCK AMORPHOUS SILICON DEPOSITION SYSTEM.

reaches an ultimate pressure of 2×10^{-7} torr, and the residual gases and their leak rates are measured with a residual gas analyzer. A multigas flow panel introduces up to eight gases simultaneously during deposition. The entire deposition sequence is controlled using an IBM PC.

2.3 SELECTION OF STARTING MATERIALS AND DETERMINATION OF FILM PURITY

To ensure ultimate film purity in our research efforts, three types of analyses are routinely performed for the selection and purity control of starting materials. These are gas chromatography/mass spectroscopic analysis of the source gases, residual gas analysis of deposition chamber background gases and their leak rates prior to deposition, and SIMS analysis of the deposited films. These are discussed separately below.

2.3.1. Gas Chromatography

The selection of starting materials and their purity control is determined using gas chromatography mass spectroscopy (GC/MS) analyses. We have found strong correlations among undesirable impurities and the surface photovoltage diffusion length measured on the films prepared with these starting gaseous materials [1]. Consequently, both doped and undoped gas sources are routinely analyzed for contaminants and rejected if necessary. Initially, the GC/MS analyses were done at RCA Laboratories where the detectability limit is $\sim$ 100ppm for their apparatus. During the latter part of this contract, a Solarex GC/MS system became operational.

The Solarex GC/MS system is shown schematically in Figure 2-2. The system is built around a computerized Hewlett-Packard turnkey GC/MS system using an HP 5890A gas chromatograph and an HP 5970 mass selective detector. The system can analyze impurities directly with an Alltech capillary column (0.35 mm FSOT, RSL-160 column coating) or with a packed column (Poropak PSAW). The detector for the packed column is a Tracor ultrasonic detector (USD) with a Shimadzu peak integrator and printer. The detectability limits should reach sub-ppm levels with the USD since it is 10^6 times more sensitive than a standard thermal detector. Quantitative analysis is routinely performed with the packed column and USD. Unambiguous identification of GC peaks are made with the mass spectrometer through a SGE jet separator. Present limits of detectability are

HP GC/MS SYSTEM

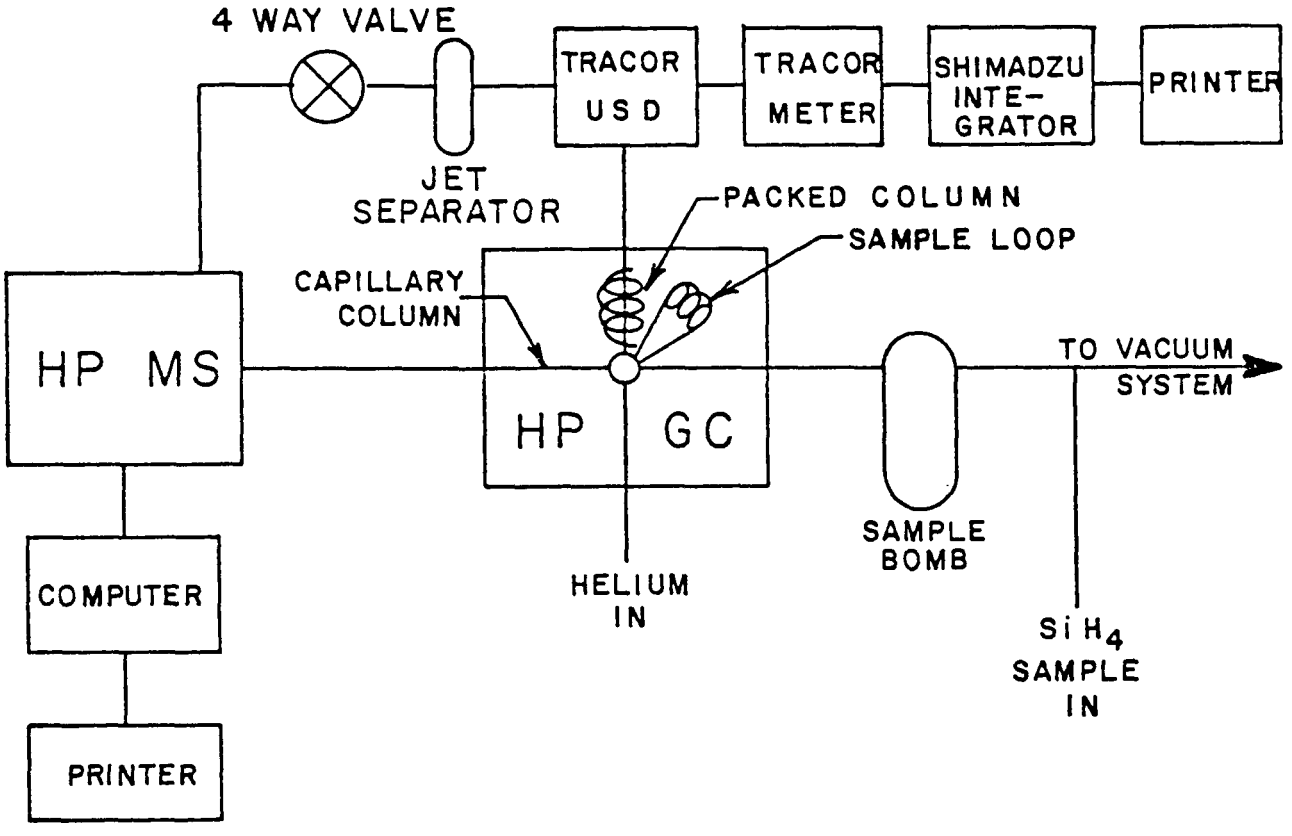

FIGURE 2-2. SCHEMATIC DIAGRAM OF THE GC/MS SYSTEM USED TO ANALYZE SILANE AND DISILANE FEEDSTOCKS.

$\sim$ 10 ppm.

The sampling system consists of a sampling bomb filled to 10 to 100 torr of gas to be analyzed. The entire system is constructed of 1/2 diameter plumbing connected with VCR fittings. The system is pumped to a base pressure of 1 x 10^{-7} torr with a 2" diffusion pump. After bakeout the leak rate (desorption rate) is $\sim$ 1 x 10^{-4} sccm. Very low leak rates are necessary to perform ppm or sub ppm analyses. External leaks are kept at less than 1 x 10^{-10} sccm. Sample injection takes place through a $1cm^3$ or 4 cm^3 sample loop.

Analytical surveys of silane and disilane were conducted for many different manufacturers and suppliers. This first survey was conducted with the capillary column and used the total ion current of the mass spectrometer as a detector. Consequently, the detectability limits were only $\sim$ 0.1% (weight).

The samples of silane analyzed at this detectability limit showed no gross impurities. A repeat of the silane survey is underway at detectability limits less than 10 ppm.

The analysis of several different samples of disilane is given in Table 2.1. All samples of disilane which were analyzed contained large amounts of impurities. Matheson disilane contained n-butane, Mitsui disilane contained ethyl silane, and Airco disilane contained $\sim$ 30% trisilane. Figures 2-3 and 2-4 shows the GC data and the mass spectra for Mitsui and Matheson disilane. Solar cells made with the Mitsui disilane had AM1 efficiencies in the 8-9% range, but the stability upon prolonged exposure was less than satisfactory ($\sim$ 50% degradation after 10^3 hours of 1 sun illumination). One example of a detrimental impurity studied in detail is disiloxane. A GC/MS analysis of a silane cylinder determined that it contained a fractional percent of disiloxane ($\sim$ 0.2%). The deposited film made from this silane cylinder had a surface photovoltage diffusion length of 0.18μm for 1 sun illumination; SIMS analysis showed that the film contained $\sim$ 1.5 x 10^{20} oxygen atoms cm^{-3}. Another film made in the same system but with a silane cylinder containing no disiloxane had a SPV diffusion length of 0.52μm; in this case the oxygen content of the film was $\sim$ 1.7 x $10^{19} cm^{-3}$. The amount of disiloxane found in silane cylinders can vary widely. Figure 2-5 shows that approximately 4% disiloxane was found in a

TABLE 2-1

Solarex GC/MS Analyses (in ppmw) of Disilane

Component	Mitsui (direct)	Mitsui (Synthatron)	Airco (Chronar)	Matheson (unknown source)
H_2	>10,000	>10,000	>10,000	100
N_2	500	600	600	300
CO_2	200	2,000	2,000	ND
Ar	ND	ND	ND	40
SiH_4	9,000	500	75,000	2,300
Si_3H_8	100	100	7,600 to 30%	1,200
Si_4H_{10}	25	25	500	ND
Siloxanes	ND	ND	<100	ND[a]
Chlorosilanes	ND	ND	<100	ND
n-butane	ND	ND	ND	3,000 to 3%
Ethyl silane	50,000	50,000	ND	ND
Propyne	<100	<100	250	ND
Unkn. #1	250	250	25	ND
Unkn. #2	10	10	200	180
Unkn. #3	ND	ND	150	ND

[a] Chlorosilanes, siloxanes, and hydrocarbons may be unknowns listed at bottom of table.

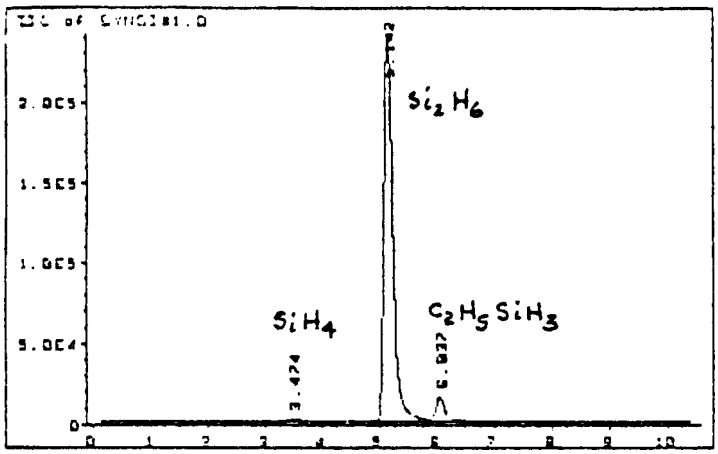

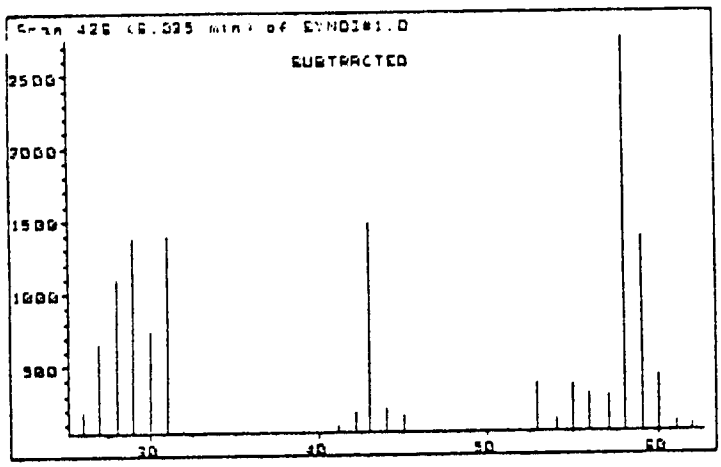

FIGURE 2-3. GC/MS DATA TO ANALYZE MITSUI DISILANE. THE TOP FIGURE IS THE RAW GC DATA AND THE BOTTOM FIGURE IS THE MASS SPECTRUM IDENTIFYING ETHYL SILANE AS A MAJOR CONTAMINANT.

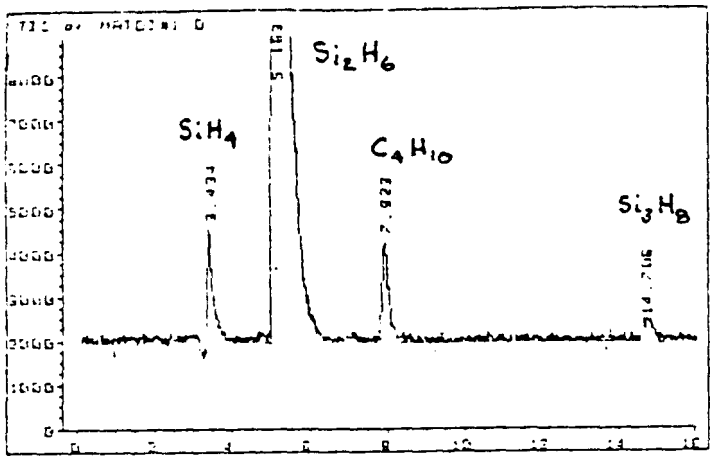

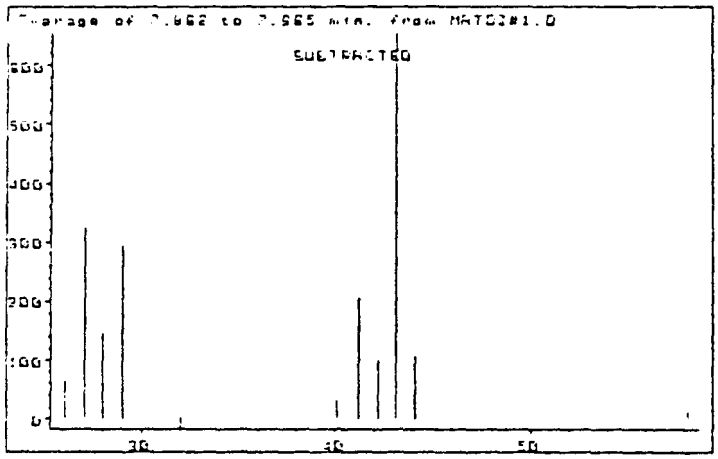

FIGURE 2-4. GC/MS DATA USED TO ANALYZE MATHESON DISILANE. THE TOP FIGURE IS THE RAW GC DATA AND THE BOTTOM FIGURE IS THE MASS SPECTRUM IDENTIFYING N-BURANE AS A MAJOR CONTAMINANT.

contaminated cylinder of silane. No observable SPV diffusion length could be measured on amorphous silicon films grown with this contaminated cylinder of silane. The top of Figure 2-5 shows a GC analysis of an uncontaminated silane cylinder which produced high quality amorphous silicon films.

2.3.2 Residual Gas Analysis

Prior to deposition, it is necessary to analyze the residual background gases and their leak rates in the vacuum system. For example, the SPV diffusion length is reduced when films are prepared with high levels of pump oils present in the vacuum system. The diffusion length is also reduced by the presence of an air leak. Thus, monitoring residual gases and their leak rates is important.

Typically, a glass bell jar system after bakeout will reach an ultimate pressure of 1×10^{-8} torr. This is limited by the inability to completely bakeout the bell jar and the outgassing of the viton "O" rings. A typical RGA analysis performed with a quadrupole mass spectrometer in a glass bell jar system is shown in Figure 2-6. The major components are H_2, H_2O, and CO. It is necessary to also measure the leak rates of each of the components of the residual gas analysis. This is because the partial pressure in equilibrium during pumping is different from the ultimate partial pressure from outgassing without pumping, i.e., gases are pumped at different rates. The total leak rate is kept at $\sim 1 \times 10^{-4}$ sccm or less for systems used to make high efficiency cells.

2.3.3 SIMS Analysis

After deposition, the impurity content of the films is determined by SIMS (secondary ion mass spectroscopy). This chemical characterization tool provides profiles or bulk determination of the hydrogen content as well as of dopants and impurities (e.g., B, P, C, O, N, Cl, F) in amorphous silicon films. Its use is especially important to monitor possible cross contamination in a multi-chamber deposition system. Finally, the impurity content in the deposited films during optimization studies can be correlated to the electronic properties and correlated to concentrations of metastable centers. Good quality amorphous silicon films typically contain $< 5 \times 10^{18} cm^{-3}$ oxygen, $< 5 \times 10^{18} cm^{-3}$ carbon, and $< 5 \times 10^{17} cm^{-3}$ nitrogen. The sensitivity limits for the SIMS apparatus are:

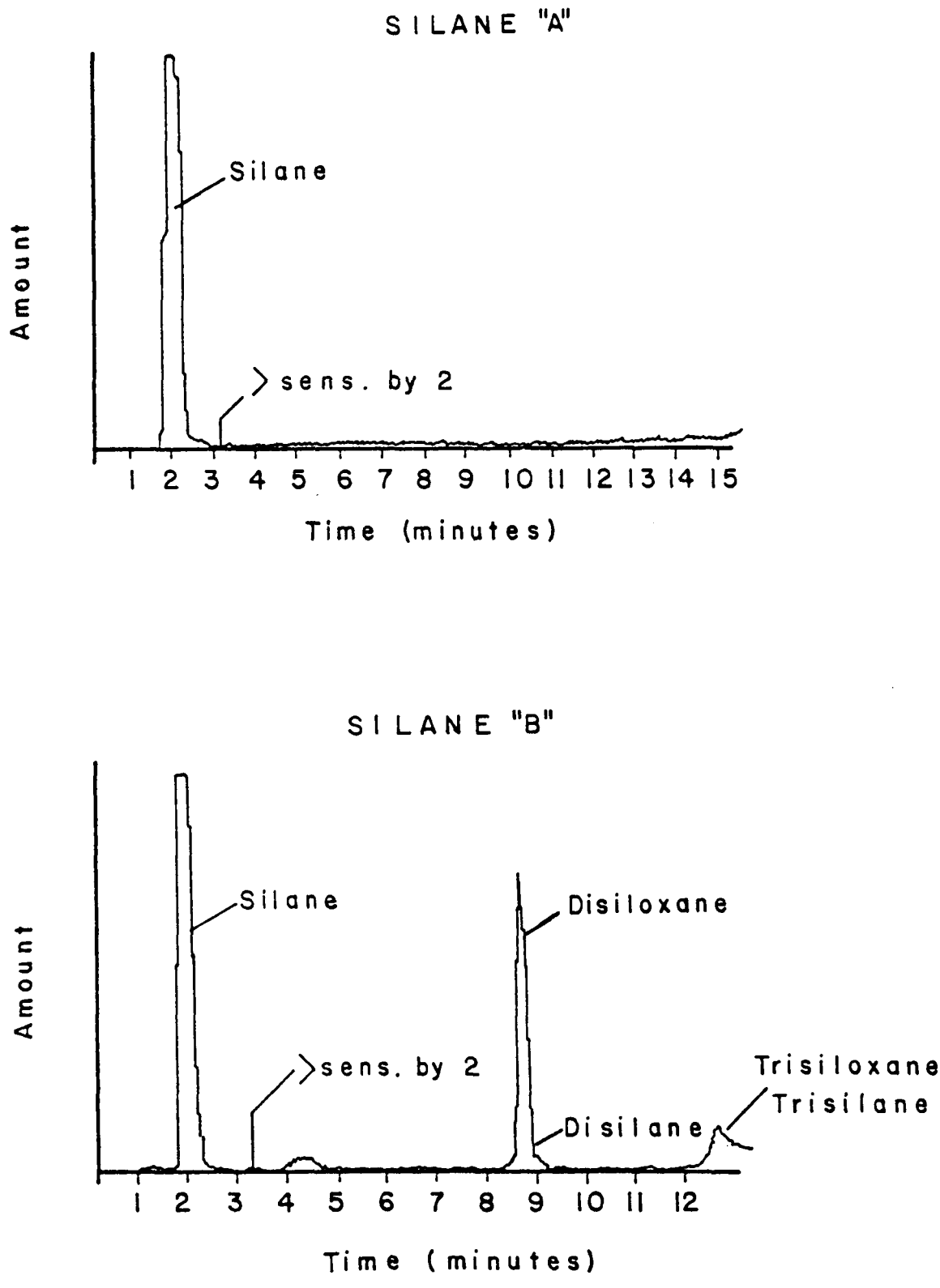

FIGURE 2-5. GAS CHROMATOGRAPH DATA FOR A SILANE CYLINDER CONTAMINATED WITH DISILOXANE (BOTTOM) AND FOR AN UNCONTAMINATED SILANE CYLINDER (TOP).

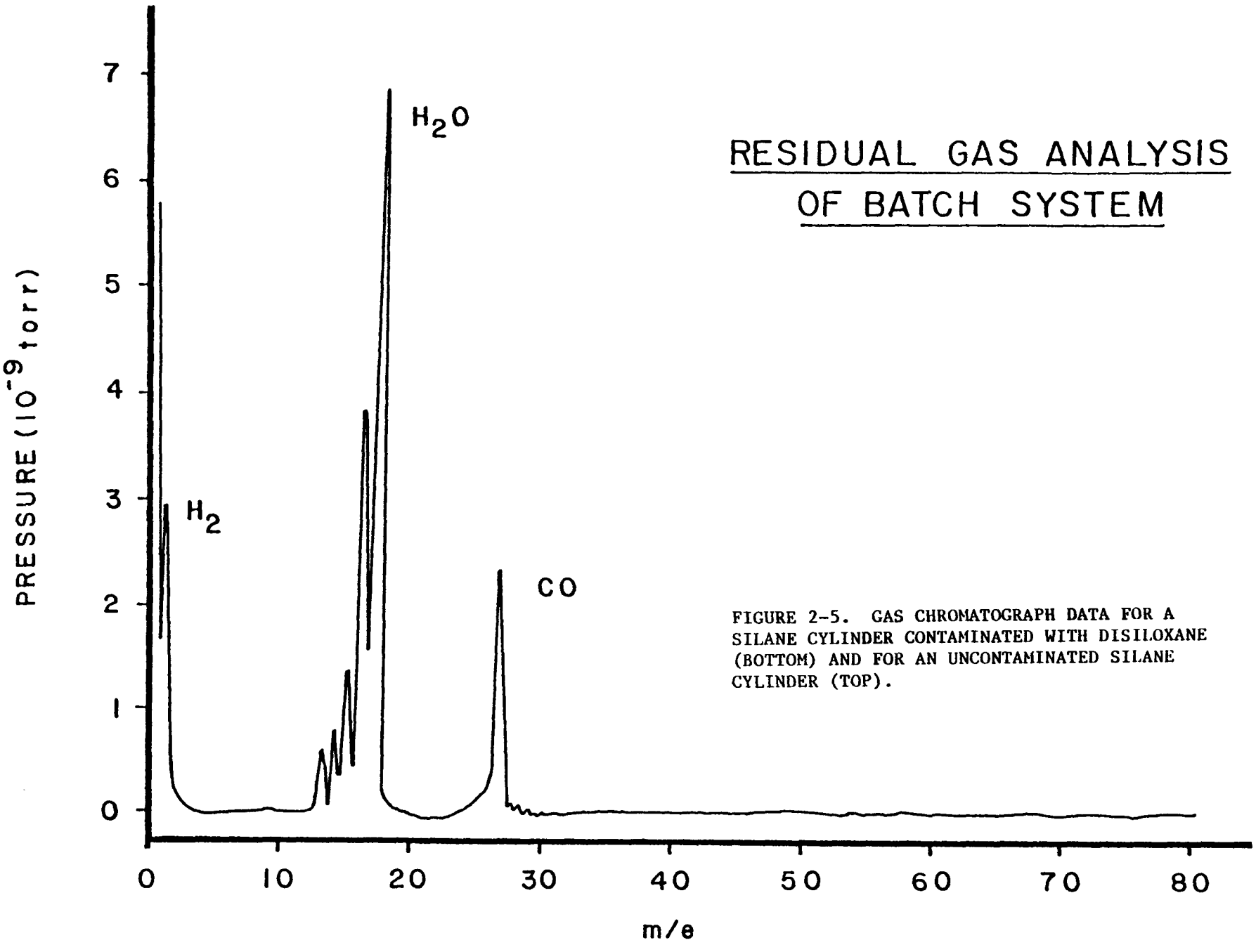

FIGURE 2-5. GAS CHROMATOGRAPH DATA FOR A SILANE CYLINDER CONTAMINATED WITH DISILOXANE (BOTTOM) AND FOR AN UNCONTAMINATED SILANE CYLINDER (TOP).

P ($\sim 10^{20} cm^{-3}$), H and O ($\sim 10^{18} cm^{-3}$), C ($\sim 3 \times 10^{17} cm^{-3}$), B and N ($\sim 5 \times 10^{16} cm^{-3}$) and C ($\sim 2 \times 10^{16} cm^{-3}$).

Figure 2-7 shows a SIMS profile of a typical p-i-n cell fabricated in the load-lock system. The oxygen ($4 \times 10^{19} cm^{-3}$) and carbon ($1 \times 10^{19} cm^{-3}$) levels are somewhat higher than the values normally observed in this system. In other films the oxygen content has been $\sim 1 \times 10^{19} cm^{-3}$, the carbon content $\sim 1.4 \times 10^{18} cm^{-3}$, and the nitrogen content $\sim 2 \times 10^{18} cm^{-3}$. As seen in Figure 2-7, recent SIMS analyses have shown residual boron contamination in the i-layer ($\sim 2 \times 10^{17} cm^{-3}$). This boron contamination level is typical of glow discharge deposition systems operating in a batch mode.

The results of SIMS analyses were used to correlated the level of impurities in the deposited films and the amount of impurities in the gas phase. The effect of these impurities on the space charge width (W_0) and SPV diffusion length (L_1) is given in Table 2-2.

The largest decrease in L_1 and W_0 are produced by adding 2% N_2 to the silane discharge. The SIMS data show that the nitrogen content of a-Si film is more than 100X larger than that observed in most of the other films. A large decrease in L_1 was also produced by adding 1% C_2H_4, and in this case, the carbon content was increased by a factor of about 20X as compared to the control film. A significant reduction in both L_1 and W_0 was caused by the presence of $\sim$0.2% disiloxane in silane; the SIMS data show an increase of about 10X in the oxygen content as compared to the control sample. Disiloxane is sometimes found as a contaminant in silane gas cylinders and readily forms when O_2 or H_2O is present in a silane glow discharge. Both oxygen and nitrogen can accidentally be introduced into the discharge atmosphere through air leaks.

Impurity gases such as CO and SiH_2Cl_2 caused some reduction in L_1 but had little effect on W_0. Since the molecular bond is very strong in the case of CO, most of the carbon and oxygen impurities may be tied up as incorporated CO molecules in the a-Si film. This conjecture is supported by the roughly comparable amounts of carbon and oxygen found by SIMS. In the case of SiH_2Cl_2, Delahoy and Griffith [2] showed that chlorine acts as a deep acceptor. Since impurities such as oxygen and nitrogen appear to create donor-like defects, the presence of

TABLE 2-2

Effects of Impurities on Diffusion Lengths

			Impurity Concentrations (cm^{-3})				
ischarge Atmosphere	L_1 (μm)	W_o (μm)	O($X10^{19}$)	C($X10^{19}$)	N($X10^{19}$)	Cl($X10^{17}$)	F($X10^{18}$)
iH_4 (control)	0.52	1.47	1.7	2.0	0.03	1.2	----
.1% SiF_4 in SiH_4	0.36	0.93	2.3	1.6	0.07	0.07	1.6
% CH_4 in SiH_4	0.32	0.83	5.2	25.0	----	0.7	----
% CF_4 in SiH_4	0.31	0.84	0.56	14.0	0.15	0.84	140
% CO in SiH_4	0.31	1.32	8.7	6.9	0.06	0.36	----
).07% SiH_2Cl_2 in SiH_4	0.30	1.56	0.3	0.3	0.15	17.0	----
0.2% $(SiH_3)_2O$ in SiH_4	0.18	0.33	15.0	0.8	1.0	1.6	----
1% C_2H_4 in SiH_4	0.15	0.77	0.25	42.0	0.26	0.08	0.3
2% N_2 in SiH_4	0.12	0.23	3.8	0.2	24.0	0.4	----

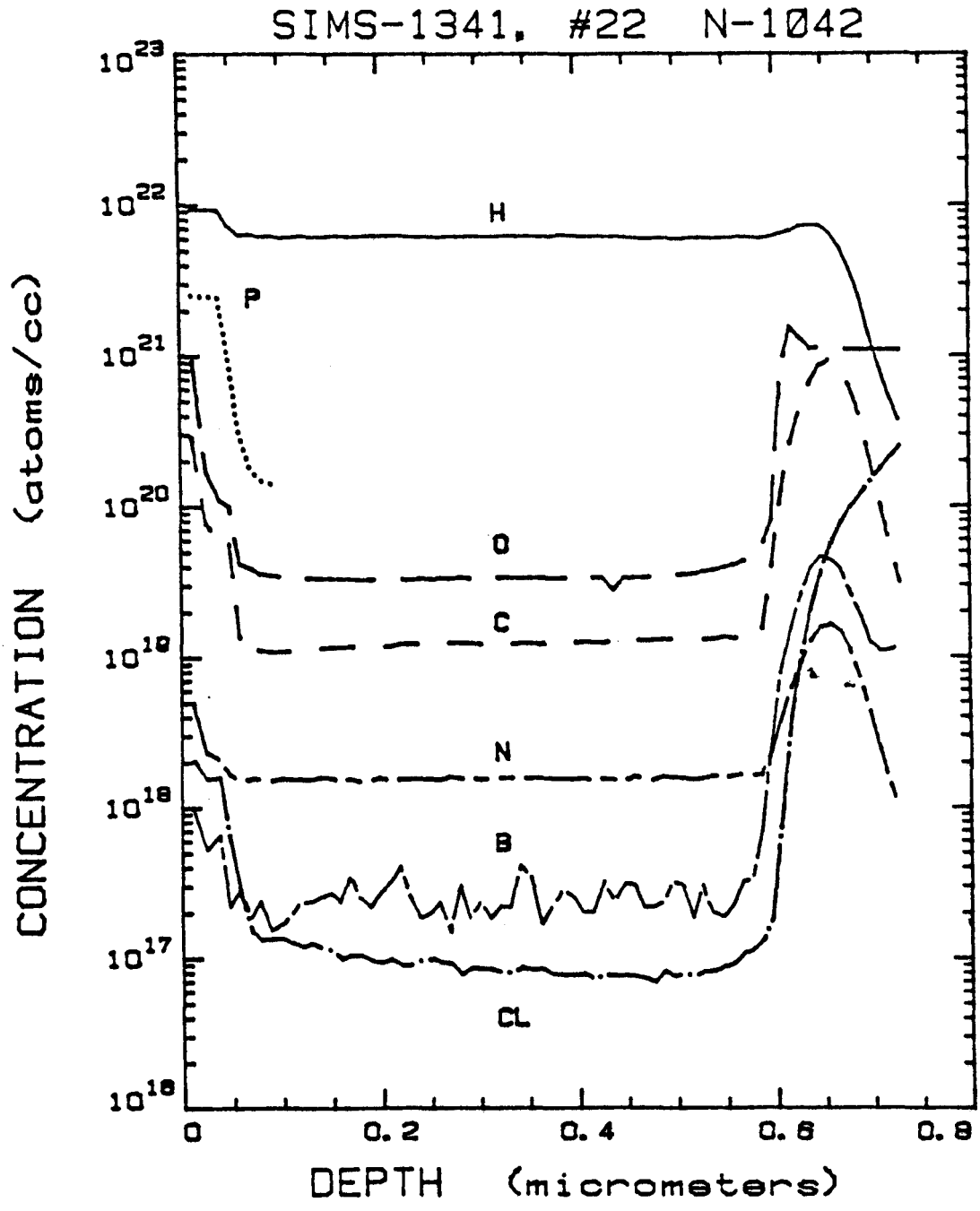

FIGURE 2-2. A SIMS COMPOSITIONAL PROFILE OF A TYPICAL P-I-N DEVICE.

chlorine may tend to compensate these other defects and thus assure a large depletion width.

The other gaseous impurities (CH_4, CF_4, and SiF_4) caused modest reductions in both L_1, and W_0. Since C_2H_4 caused a large decrease in L_1, the nature of the defect appears to depend on the source of the carbon impurity. Tawada et al. [3] came to a similar conclusion in comparing CH_4 and C_2H_4 as feedstocks for producing p-type a-Si:C:H films.

2.4 EFFECTS OF DEPOSITION RATE ON FILM PROPERTIES

Because the deposition rate is determined by the deposition parameters, one must consider a multi-dimensional approach to increasing the deposition rate. The deposition parameters that affect the deposition rate (r_d) are electrode separation distance (d), total pressure (p), substrate temperature (T_s), current density (j), the resulting maintenance voltage (V_m), and total gas flow rate (f). For rf systems the power input is measured instead of the current density and the resulting maintenance voltage. In addition, the gas composition affects the rate of deposition. To economically produce large area cells in a multi-chamber system, the silane must be utilized efficiently, and this is being determined for the above matrix of deposition parameters and resulting deposition rates.

The deposition rate is being measured by making doped and undoped amorphous silicon depositions for a fixed time interval. The resulting film thickness is measured with a scanning profilometer over a film step made by etching away part of the a-Si:H film. Because the type of substrate affects the deposition rate, various substrates such as quartz, stainless steel, and transparent conducting oxides are being used when measuring deposition rates for the above matrix of deposition parameters.

To correlate the effects of deposition rate and deposition parameters on film quality, constant SPV diffusion length measurements are being made before and after extended illumination. We have obtained diffusion lengths as large as 0.64μm after 48 hours of AM1 illumination for films grown in an rf glow-discharge deposition system at a rate of 9.6nm/min. Increasing the deposition rate to 68nm/min resulted in a diffusion length of 0.40μm after 48 hours of light soaking.

Figure 2-8 shows the variation in diffusion length with rf power density for a series of films grown at Vactronics under Subcontract STF-1. The deposition rate varied from 18nm/min at a power density of 80mW/cm^2 to 68nm/min for 250mW/cm^2. The films were grown on stainless steel substrates (except for the film grown at 80mW/cm^2 where the substrate was indium-oxide coated glass). The data in Fig. 2-8 indicate that the initial SPV diffusion lengths (before light soaking) increase with increasing rf power (or deposition rate). After 48 hours of AM1 illumination, the data indicate that the best films are made at the lowest power densities. The large effect of light soaking on films made at high powers suggests that space-charge effects are contributing to the initial SPV measurements.

Optical absorption measurements show that the optical gap increases from 1.78eV to 1.91eV as the deposition rate increases from 54 to 168nm/min. Earlier work with rf electrodeless discharges showed a similar effect as the hydrogen content increased with increasing rf power [4].

Figure 2-9 shows how the deposition rate varies as the hydrogen content of the discharge atmosphere varies. At an rf power density of 150mW/cm^2, the maximum deposition rate is 6Å/s at a composition of $\sim$25% SiH_4, while at a power density of 225mW/cm^2, the maximum rate is 12Å/s at $\sim$40% SiH_4.

2.5 STABILITY OF AMORPHOUS SILICON FILMS UNDER OPTICAL ILLUMINATION

2.5.1 Stability Studies

We have started to perform routine stability tests on both a-Si:H material and p-i-n solar cells (see Section 4.0). For studying the stability of a-Si:H material, we are measuring the diffusion length and space-charge density before and after light soaking (see Fig. 2-8). In some cases, we are fabricating p-i-n devices and measure both the I-V characteristics and the quantum efficiency before and after light soaking. These data are analyzed to give an estimate of the collection length under illumination. Both a-Si:H material and devices are being light-soaked under constant 1 sun illumination, and we are using both tungsten-halogen and sodium vapor lamps as light sources.

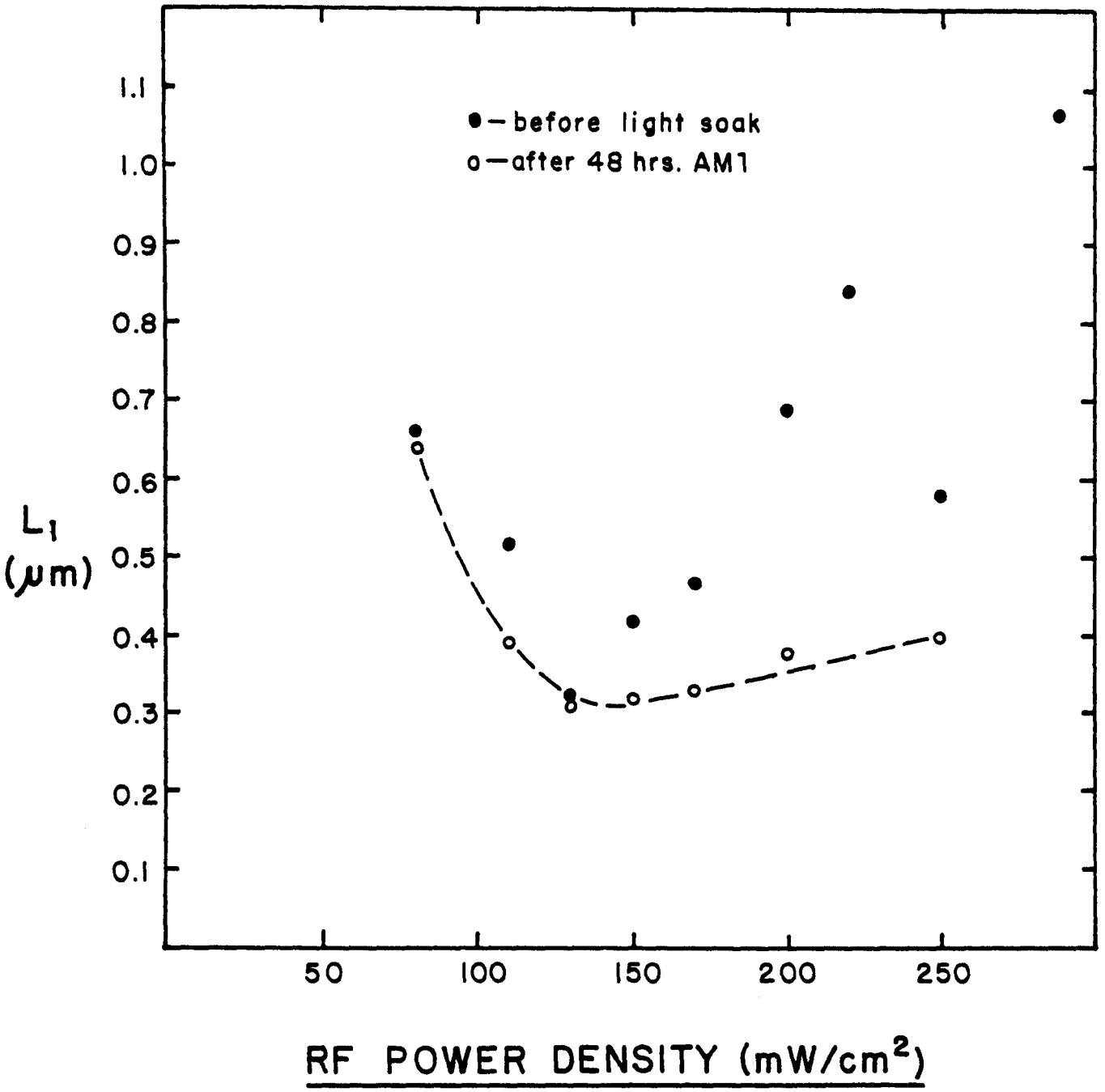

FIGURE 2-8. SPV DIFFUSION LENGTH AS A FUNCTION OF RF POWER DENSITY.

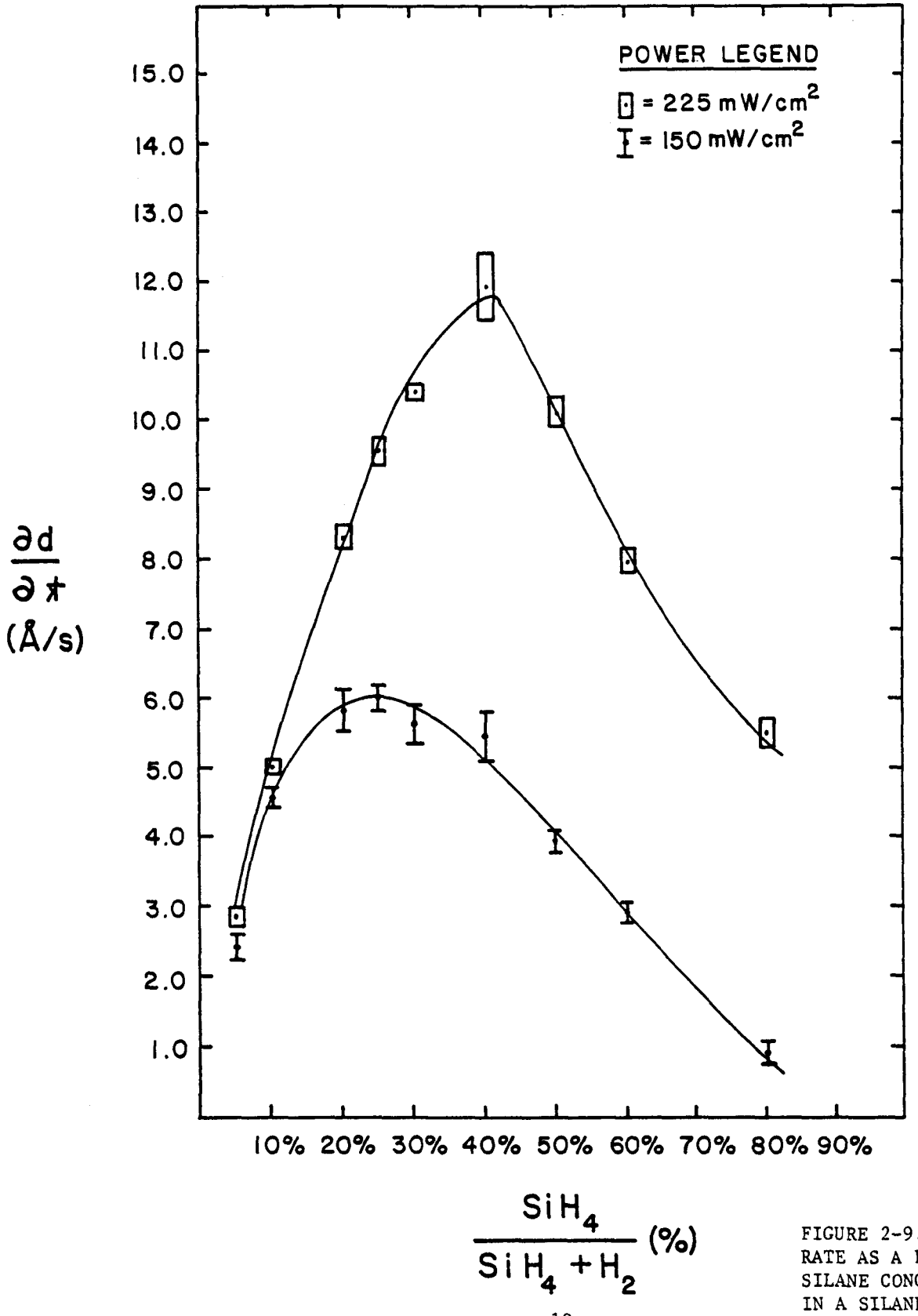

FIGURE 2-9. DEPOSITION RATE AS A FUNCTION OF SILANE CONCENTRATION IN A SILANE-HYDROGEN DISCHARGE.

The diffusion length is measured by the surface-photovoltage method (SPV). In this technique the diffusion length is measured by varying the wavelength of incident light and adjusting the photon flux to assure a constant photovoltage. The degradation of diffusion length with time is summarized in Table 2-3. The samples SE 0 to SE 4 are i-layers deposited at rates between 4 to 6Å/s by rf glow discharge and the samples C12144A1 to C12144A4 are i-layers deposited at rates 4 to 5Å/s by dc glow discharge process. Some samples, particularly SE 3 and SE 4 have high initial values of diffusion length (as high as 0.69μm) which degrade to 0.38μm after 48 hours of AM1 illumination. Another sample C12144A3 which has an initial diffusion length of 0.38μm degrade to only 0.36μm after 48 hours of illumination.

2.5.2 Analysis of Mechanisms

Recent results indicate that impurities such as oxygen [5] and carbon [6] can create metastable centers in a-Si:H. Moreover, some preliminary data indicate that the concentration of metastable centers depends strongly on the source of the contaminant (e.g., CO vs CH_4) as well as on deposition conditions.

However, some metastable centers appear to be associated with microstructural defects [7]. We still see light-induced effects in a-Si:H films and a-Si:H solar cells even when the total impurity content is $\lesssim 10^{19} cm^{-3}$. In general, we find that the stability improves when the hydrogen content is reduced, either by increasing the deposition temperature (for Schottky devices on stainless steel) or by decreasing the rf power (see Fig. 2-8). The role of hydrogen is supported by the observation of reversible, electron-beam-induced degradation of hydrogenated grain boundaries in polycrystalline silicon [8].

2.6 MEASUREMENT OF ELECTRONIC AND OPTICAL PROPERTIES

An important electronic characterization tool is the constant surface photovoltage technique for determining minority carrier diffusion lengths. We are using this tool to monitor the electronic quality of a-Si:H films produced under various deposition conditions as we attempt to continue improving the quality of these films. Presently, the apparatus measures the minority carrier diffusion length under 1 sun illumination and the space charge density in the

TABLE 2-3

DEGRADATION OF DIFFUSION LENGTHS

Sample #	L_1 (μm) Initial Value	L_1 (μm) After 48 hrs AM1
SE0	0.32	0.31
SE1	0.47	0.33
SE2	0.52	0.39
SE3	0.69	0.38
SE4	0.61	0.36
C12144A1	0.33	0.28
C12144A2	0.28	0.21
C12144A3	0.38	0.36
C12144A4	0.31	0.25

dark. As mentioned above, we are currently measuring diffusion lengths of ~ 0.6 μm for undoped a-Si:H films.

Another important electronic characterization is the measurement of conductivity, especially for doped films. The 4 point probe apparatus presently being used measures conductivities as low as 10^{-11} to 10^{-12} $(\Omega\text{-cm})^{-1}$. Activation energies are determined from the temperature dependence of the conductivity. An example of an important electronic characterization is the adjustment of the resistivity of the boron-doped p-layer containing various amounts of carbon to open the bandgap. Experimentally, 200 - 300Å thick p-layers are grown with varying amounts of methane. The optical gap is measured from absorption measurements and the resistivity is measured from absorption measurements and the resistivity is measured with the 4-probe device. Generally, the largest bandgap with the smallest resistivity is desired and a tradeoff occurs for optimum cell performance. A typical optimization of a p-layer is shown in Fig. 2-10 for films deposited in a dc glow discharge.

Optical absorption measurements are necessary to determine the bandgap of the deposited doped and undoped films. The Tauc coefficients (C, E_g), as determined from $(\alpha h\nu)^{\frac{1}{2}} = C(h\nu - E_g)$, are needed for input to the constant SPV diffusion length measurements. A determination of the Tauc coefficients is shown for an undoped amorphous silicon film in Fig. 2-11. It is desirable to make optical measurements on thick ($\sim 1.5\mu m$) and on thin ($\sim 0.5\mu m$) films to obtain data for SPV diffusion length measurements. Often the thick films show band-tailing and can lead to incorrect extrapolations.

Figure 2-12 shows the variation in the resistivity of undoped a-Si:H as the hydrogen content of the rf discharge atmosphere is varied. Generally, good transport properties for solar cells are only attained when $\rho > 10^8$ Ω-cm. The data in Figure 2-12 suggest that microcrystallites may be present when the silane concentration is less than $\sim 20\%$. Other investigators have shown that microcrystalline Si:H can form when silane is highly diluted in hydrogen, especially at high rf power densities [9].

Another measurement essential to optimize both doped and undoped films is the determination of quantum efficiency as a function of wavelength. These

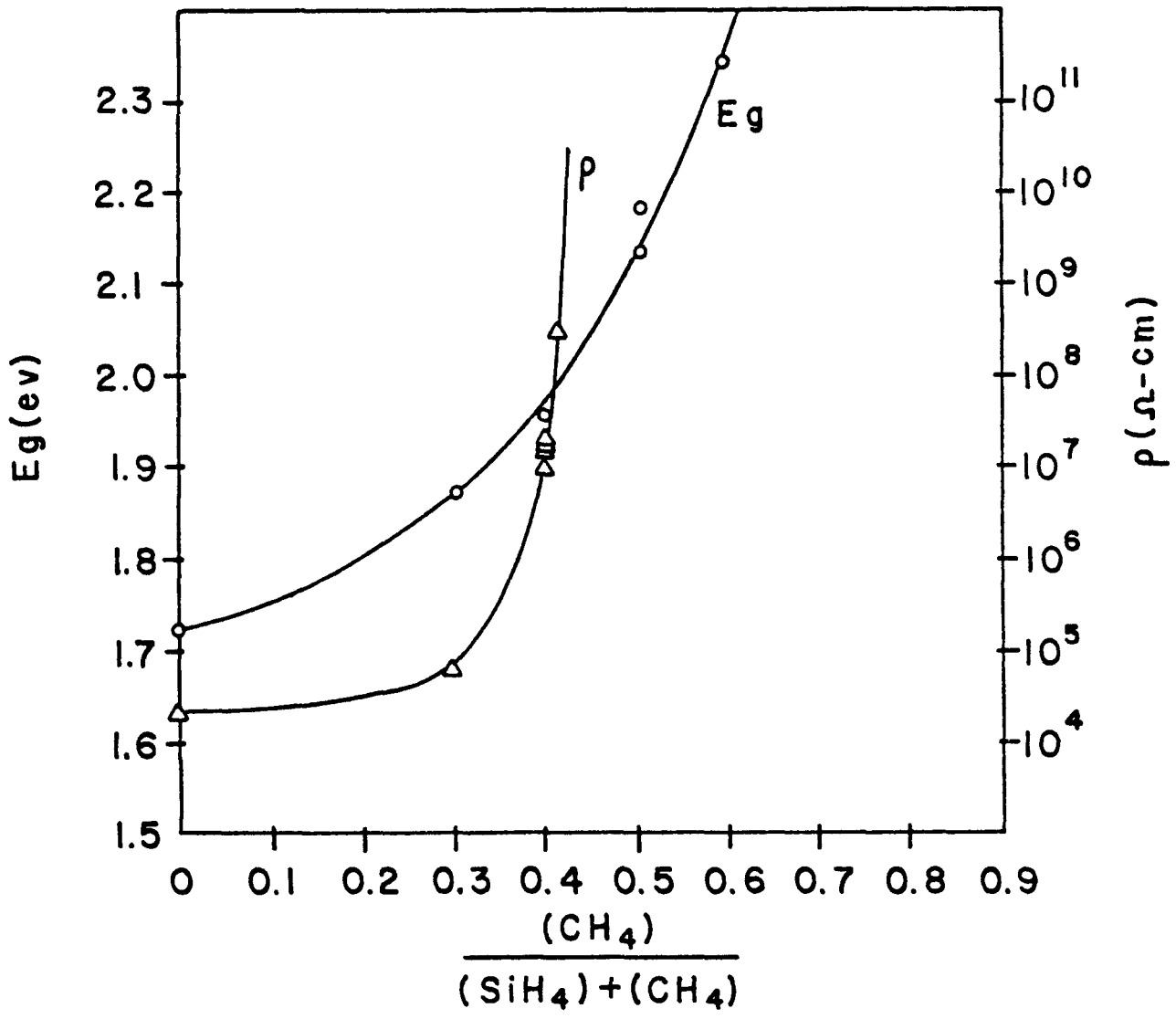

FIGURE 2-10. THE OTPICAL GAP AND RESISTIVITY OF BORON-DOPED (0.2% B_2H_6) a-Si:C:H AS A FUNCTION OF METHANE CONCENTRATION.

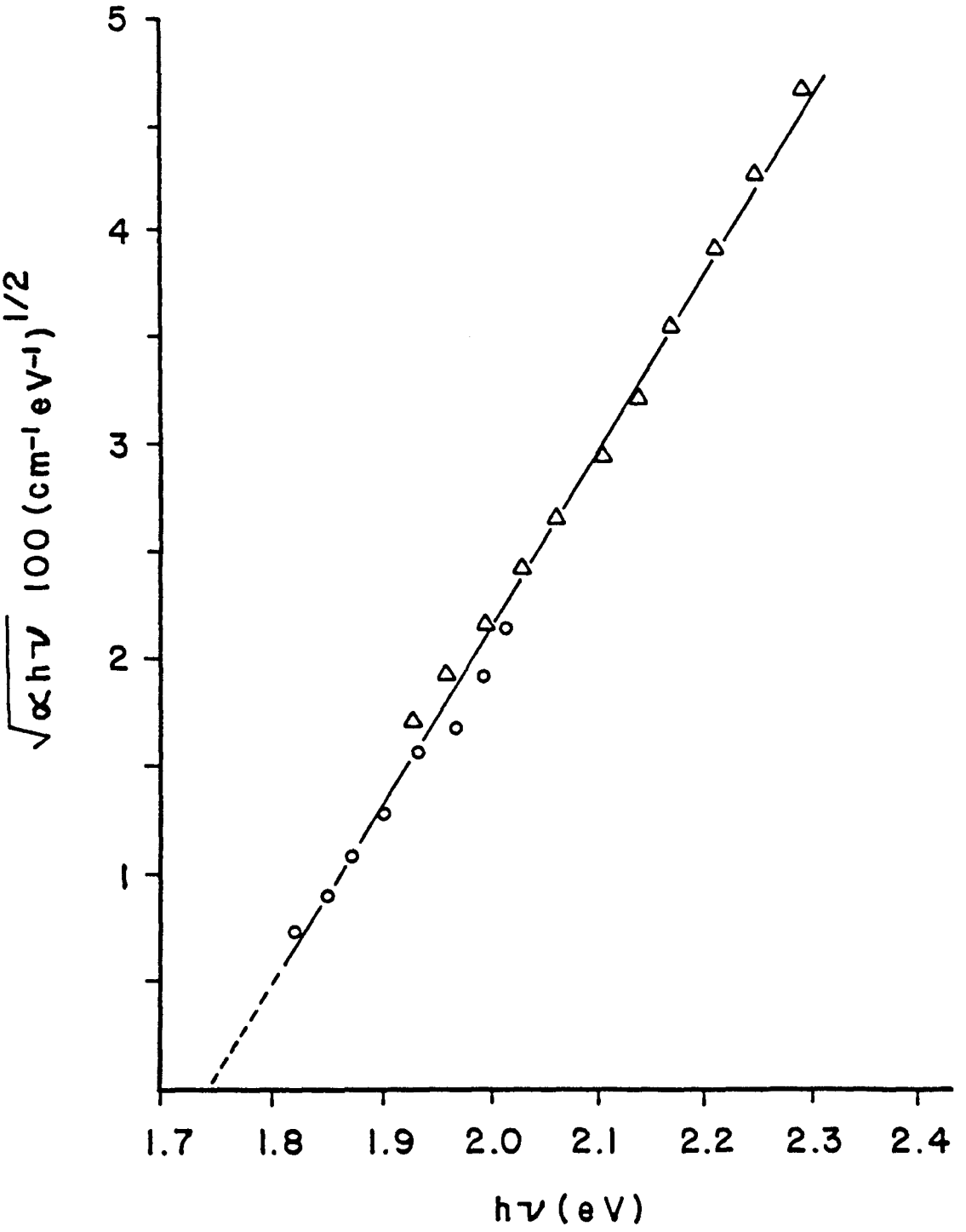

FIGURE 2-11. PLOT USED TO DETERMINE THE TAUC COEFFICIENTS FROM THE OPTICAL ABSORPTION DATA FOR I-LAYERS OF TWO THICKNESSES: 1.5μm(O) and 0.5μm (Δ)

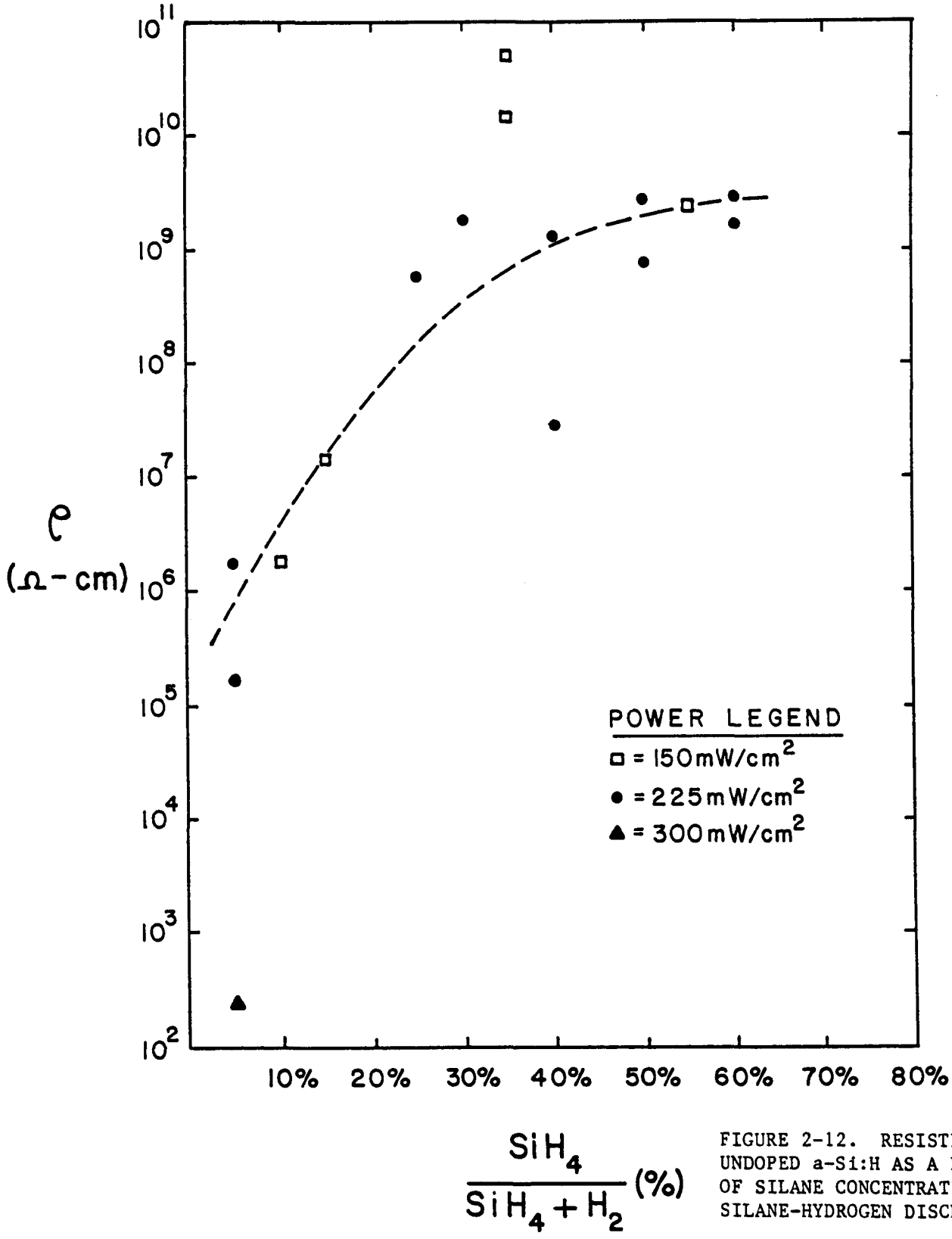

FIGURE 2-12. RESISTIVITY OF UNDOPED a-Si:H AS A FUNCTION OF SILANE CONCENTRATION IN A SILANE-HYDROGEN DISCHARGE.

measurements serve as a diagnostic in solar cell performance. For example, the spectral response is used to monitor the p-layer window performance in p-i-n structures. The quality of the i-layer under extended illumination can be determined by monitoring the performance of Schottky barrier cells. The changes in FF, η , J_{sc}, and V_{oc} can be determined under extended illumination. These measurements have proven to be a rapid way of screening i-layers prepared under various deposition conditions. Finally, the collection length as determined from quantum efficiency measurements can be correlated to the constant SPV diffusion length.

Table 2-4 summarizes the deposition parameters and properties of a-Si:H films currently being used in solar cells with conversion efficiencies of 8 - 10.5%.

TABLE 2-4

DEPOSITION PARAMETERS AND PROPERTIES OF OPTIMIZED AMORPHOUS SILICON FILMS

dc GLOW DISCHARGE

a-Si:H	Discharge Atmosphere	ε_{opt} (eV)	$\sigma_d(\Omega^{-1}cm^{-1})$	$\sigma_p(\Omega^{-1}cm^{-1})$
p-layer	0.2%B_2H_6, 50%CH_4, 50%SiH_4 (100 sccm)	1.92	3×10^{-6}	10^{-6}
i-layer	100% SiH_4 (100 sccm)	1.67	10^{-10}	10^{-4}
n-layer	1.8%PH_3 in SiH_4 (140 sccm)	1.7	10^{-2}	-

NOTE: T_s = 240°C, dc current density ≅0.13mA/cm^2 and pressure ≅0.5Torr for all 3 layers.

rf GLOW DISCHARGE

a-Si:H	Discharge Atmosphere	ε_{opt} (eV)	$\sigma_d(\Omega^{-1}cm^{-1})$	$\sigma_p(\Omega^{-1}cm^{-1})$
p-layer	0.18%B_2H_6, 50% CH_4, 50%SiH_4 (200 sccm)	2.05	10^{-7}	10^{-6}
i-layer	100%SiH_4 (200 sccm)	1.71	10^{-9}	10^{-4}
n-layer	1%PH_3 in SiH_4 (160 sccm)	1.7	10^{-2}	-

NOTE: T_s = 230°C, pressure = 0.5 Torr, rf power 50mW/cm^2 for all 3 layers.

σ_p is measured under simulated 1 sun illumination.

2.7 STATUS OF ANALYTICAL FACILITIES

All equipment required for material characterization became operational during this contract on or ahead of schedule.

A table summarizing facilities is given in Table 2-5.

TABLE 2-5

SUMMARY OF CHARACTERIZATION FACILITIES

Characterization Equipment	Quantity Measured	Location	Status
SIMS	impurity and doping profiles	RCA	operational
DLTS	density of gap states	RCA	operational
GC/MS	gas impurities	Solarex	operational
Spectral Response	absorption coefficients, bandgaps	Solarex	operational
Surface Photovoltage	diffusion length, depletion width	Solarex	operational
Current-Voltage Apparatus	dark conductivity, activation energy, photoconductivity	Solarex	operational
Light Soaking Apparatus	all photovoltaic parameters	Solarex	operational

SECTION 3.0

TASK NO. 2: NON-SEMICONDUCTOR MATERIALS RESEARCH

3.1 INTRODUCTION

The goal of this task is to investigate and improve the structural, chemical, electronic and optical properties of the non-semiconductor materials required for optimum utilization and solar-cell performance of the amorphous silicon materials prepared in Task 1. As seen in Fig. 3-1, six different layers or structures comprise the set of non-semiconductor materials required for various aspects of the function and performance of the solar-cell module. The efficiency, stability, and durability of the cell is affected by each of these materials and structures as well as by their method of preparation.

The reasoning behind selections made, options available, and progress in material and process development accomplished during the first year of this subcontract are outlined below. Table 3-1 summarizes the selections of materials and progress to date.

3.2 MATERIALS SELECTION AND PREPARATIONS

3.2.1 Substrate Selection and Preparation

The simplest, most available, and lowest cost substrate is float made, soda-lime glass. For moderate size modules of about 1 ft square, 1/8" thickness should provide adequate strength, and in most environments little or no degree of temper is required. Commercial glass of this thickness is readily available at about 0.35$/ft. The transmission in the visible relative to air is about 87% including about 3% absorption which is due mostly to the iron content of this glass. The major advantages are the low cost and universal availability. Disadvantages are the relatively low transmission and the high impurity content.

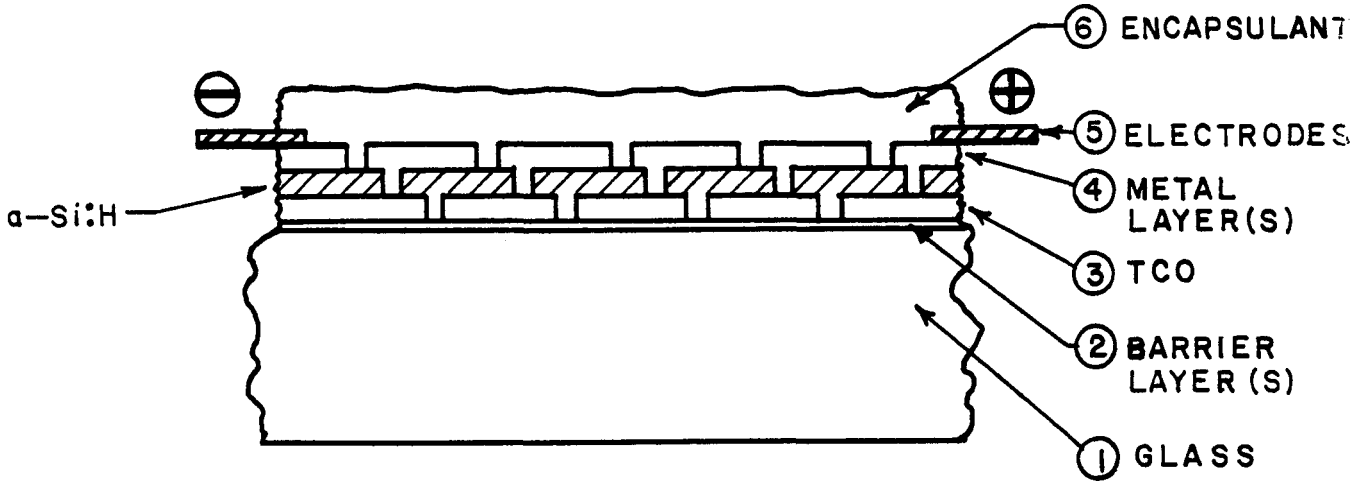

FIGURE 3-1. A SCHEMATIC DIAGRAM OF THE a-Si:H SOLAR-CELL STRUCTURE.

TABLE 3-1
TASK 2: Non-Semiconductor Materials

Subtask	Selection	Preparation (Progress)	Comments
(a) Substrate selection and preparation	Primary - float-glass, sodalime, 1/8" thickness, untempered Options: low iron, textured front and/or back	cleaning station purchased & assembled, method qualified. Ultrasonic tank rinse and freon dry.	degree of temper required still uncertain, may require 3/16" thickness. cost/availability under investigation.
(b) Preparation, Characterization, and Optimization of TCO	Primary - SnO_2 process CVD textured structure $R_{\square} \cong 10\ \Omega/\square$ thickness $\cong$ 6000Å	commercial CVD belt furnace specified, tested, and received. Laboratory belt furnace constructed and operational. Samples prepared for deliverables.	In laboratory furnace, textured SnO_2 films were made on $\geq 400cm^2$ with $R_{\square} \leq 25\ \Omega/\square$ A 10.5% cell was made on textured SnO_2. WJ furnace was tested and SnO_2/SiO_2 films of $10\ \Omega/\square$ with $\alpha < 10\%$ were made.
(c) AR films	Primary - none other than SnO_2 Options - textured glass	textured glass sample acquired	Cost vs. effectiveness will be evaluated
(d) Interface glass/TCO	Primary - SiO_2 thickness 1000-2000Å preparation - CVD	deposition head for laboratory belt furnace completed. SiO_2 head in commercial CVD belt furnace	SiO_2/SnO_2 on sodalime glass was demonstrated with commercial CVD belt furnace.
(e) Preparation, Characterization and Optimization of Metallization	Primary - Al DC magnetron sputtering thickness 5000Å Options - Ti/Al, Mg/Al	laboratory sputtering system (S-gun) assembled and operational. RF diode in-line system operational. High throughput DC magnetron system under construction and 98% complete.	High throughput demonstrated for $1000cm^2$ with dc magnetron system. Rate was 20/hr for 4000Å of aluminum on $1ft^2$.
(f) Interfaces TCO/a-Si/Metal	under investigation		
(g) Encapsulation	Primary - EVA/Tedlar 0.018"/0.004" lamination Options - Thin Film (Tedlar) adhesive - roll-on	Commercial laminator, Spire 240 purchased; installation operational. Laboratory laminator operational.	Chosen because of existing body of knowledge and extensive testing. EVA thickness will be minimized. Materials and process under development in conjunction with DuPont Polymer Film

A growing number of glass manufacturers now recognize the needs of the solar industry and offer forms of low iron glass at reasonably attractive prices. For example, Guardian Industries[+] sells a low iron solar glass which has a transmission (400-1000nm) of 91% for 1/8" thickness. They also provide an optional single surface etch which reduces the sun-side reflection by 75%, resulting in a net 94% transmittance.

The alkali content (sodium and potassium) in soda-lime glass has an adverse effect on the subsequent deposition of the TCO by high temperature processes, often preventing nucleation of the film or causing voids. In addition, slow-diffusion of impurities from the glass could cause degradation of the solar-cell module. For these reasons, we have chosen to include a buffer layer of SiO_2 between the glass and the SnO_2 conductive oxide.

It is anticipated that for production rates of less than 1MW/yr, the glass will be purchased precut to size and preparation will consist of cleaning and drying. For large-scale production, lower costs may be obtained by purchasing bulk quantities of glass in large sheets and cutting to size before cleaning. For low production rates, batch cleaning is sufficient to match the product flow. Such cleaning consists of successive tanks utilizing ultrasonic cleaning with biodegradable soap, followed by cascade rinsing and freon vapor drying stations. This type of system has been purchased, assembled, and is in use for this program. For high production rates, the cleaning and drying will be done in an in-line glass washer. Such machines are capable of cleaning rates in excess of 500 linear ft/hr and in widths up to six feet. The Solarex Thin Film Division has acquired a Bilco[++] washer (Series 300) and plans to use it in later phases of this work.

[+]Guardian Industries, Solar Glass Division, 1901 Raymer St., Fullerton, CA 92633.

[++]Bilco Manufacturing Inc., Grandview Blvd., Zelienople, PA 16063.

3.2.2 Preparation, Characterization, and Optimization of TCO

The desired properties of the TCO and the system for deposition are:

(i) Sheet resistance $R_{\square} \leq 10\ \Omega/\square$
(ii) Optical absorption $\leq 5\%$
(iii) Provide a compatible interface with a-Si
(iv) Provide good optical coupling to a-Si cell
(v) Compatible with laser scribing
(vi) Ease of ohmic contact with chosen metals
(vii) Deposition system should provide the above TCO properties, and be capable of high production rates.

To optimize the TCO in accordance with the above requirements, we have surveyed and experimentally evaluated several techniques for the deposition of conductive oxides. These include: sputtering, pyrolytic spraying, and atmospheric CVD. For the chosen oxide, SnO_2:F, we have concluded that atmospheric CVD in a belt furnace provides the best means of achieving the desired properties. In our evaluation program, we were able to chemically vapor deposit SnO_2:F films with sheet resistances $< 20\ \Omega/\square$ and otpical absorption losses of $\sim 15\%$. Sprayed tin oxide films exhibited somewhat higher absorption losses ($\sim 25\%$) for comparable sheet resistivities and were generally less uniform than CVD films. Sputtered films were generally more resistive ($> 100\ \Omega/\square$) for comparable film thicknesses ($\sim 0.2 - 0.4\mu m$).

Early in this program, we concluded that the commercially available Watkins-Johnson[+] CVD belt furnace could provide SnO_2 coatings on the chosen glass substrate adequately satisfying all but two of the desired conditions. Examinations and experiments have shown that films prepared by CVD have high conductivity ($\sim 3\text{-}4 \times 10^{-4}\ \Omega$-cm), have low absorption, are compatible with a-Si cell structures including laser scribing, and make low resistance ohmic contact to both p-layers ($1\ \Omega.cm^2$) and several metals ($10^{-3}\ \Omega.cm^2$). For higher efficiency cells, improvements will be needed in the optical coupling to the amorphous silicon. Also, we feel that the projected throughput (estimate by Watkins-Johnson) of about 30 ft^2/m could be increased.

[+]Watkins-Johnson, 440 Kings Village Road, Scotts Valley, CA 95066.

In addition to setting up a commercial belt furnace, the Solarex Thin Film Division has undertaken a development program to study the CVD deposition of SnO_2:F in a laboratory belt furnace. For this purpose, a small furnace with a 12" belt was constructed having two CVD heads, one for SiO_2 and one for SnO_2. The construction was completed in the first quarter, and SnO_2 films were made and examined during the second quarter. Pyrex (7059) substrates of up to 8" square (400cm^2 area) have been coated. Solar cells have been made on 3" square coated substrates, with conversion efficiencies up to 10.5% (see Section 4.2). We are presently producing SnO_2:F films with an optical absorption of $\sim$10-15%, a sheet resistance of $\sim$10-25 $\Omega/\square$ and a thickness of $\sim$0.6μm. Since the tin oxide is textured (see Fig. 3-2), the optical absorption is measured using an integrating sphere.

3.2.3 Anti-Reflection Films

A flat glass plate will reflect 4% of the incident light. When cost is of no major concern, reflection over a large portion of the visible bandwidth can be significantly reduced by application of multi-layer, anti-reflection coatings. However, at projected costs for PV modules of less than 0.50$/watt, only 0.02$/watt or about 20 cents/ft^2 can be allocated to remove reflections. With this cost constraint and because of the minor nature of this problem, only simple, low-cost methods will be briefly explored. We have acquired some glass samples with a front surface etch that reduces reflection, and we will be using these substrates to fabricate some high performance amorphous silicon solar cells. The reflection from the glass/SnO_2/p-i-n/Al structure is relatively small since the SnO_2 affords good optical coupling into the a-Si:H.

3.2.4 Interface Between Substrate and TCO

If the lowest cost sodalime glass is to be used as a substrate, the impurities resident in such glass must be considered. The major potential problems are:

1. Interaction of outgassing impurities and mobile ions with nucleation of TCO films during high temperature (500°C) processing.
2. Possible long term degradation of the solar cell.

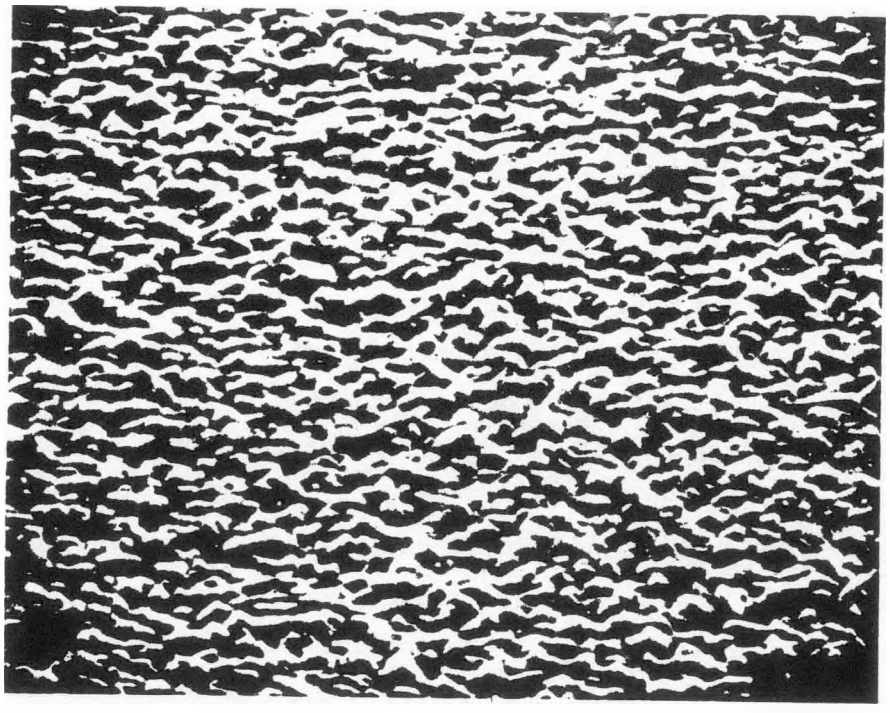

FIGURE 3-2. SEM PHOTOGRAPH OF TEXTURED TIN OXIDE ON QUARTZ (MAGNIFICATION IS 10^4X; 45° ANGLE).

The first is of immediate concern because SnO_2 films will not form on high temperature sodalime glass surface unless they are specially treated or a buffer layer is provided. Acid leaching of soda glass can result in reasonably good SnO_2 films, but microvoids and large surface defects remain. A buffer layer provides a more reliable and reproducible surface, and significantly reduces long term diffusion of impurities from the glass both during processing and afterwards.

We have chosen SiO_2 as the buffer. A film of 1000-2000Å thickness has provided an adequate nucleation surface for CVD deposited SnO_2 and should be of sufficiently thick to act as a barrier for diffusion. The Watkins-Johnson CVD belt furnace has one SiO_2 deposition head followed by two SnO_2 heads. We have also included an SiO_2 deposition head in our laboratory belt furnace.

3.2.5 Interfaces Between TCO/a-Si:H and a-Si:H/Metal

Preliminary data indicate that the tin oxide/a-Si:H interface degrades if the substrate temperature exceeds about 280°C. Degradation of the interface can occur at even lower substrate temperatures if the discharge atmosphere is rich in hydrogen. Auger electron spectroscopy of the interface region indicates that the degradation is related to the reduction of the tin oxide and the formation of silicon oxides.

Generally, we do not encounter difficulties with the a-Si:H/metal interface. However, if the a-Si:H structure is exposed to air while still hot (100°C), it is possible to develop an oxide layer that will inhibit the formation of an ohmic contact. Moreover, if Al is used as the back contact, the solar cell must not be subjected to temperatures > 150°C since interdiffusion of Al and Si can induce crystallization [10].

3.2.6 Preparation, Characterization, and Optimization of Metallization

We have been metallizing the a-Si:H cells using an in-line sputtering system, an S-gun batch system and an electron-beam evaporation system. We are able to deposit metals such as Al, Ti, Mg and Ni over areas of $1000cm^2$. We have demonstrated the deposition of 4000Å of Al in 2.5 minutes using an in-line DC

magnetron system. The contact resistance for Al deposited on n-type a-Si:H is generally $< 0.5\,\Omega\text{-cm}^2$.

Good ohmic contacts to n-type a-Si:H and to tin oxide can be obtained by either sputtering or electron beam evaporating metals such as Al, Ti and Mg. Sputtering has an advantage in assuring reliable contacts since the more energetic species present in a sputtering discharge can penetrate thin oxide or contamination layers. Moreover, sputtering can provide more uniform coverage for continuous, in-line coating of large area substrates. Both techniques are capable of depositing metals rapidly (> 2000Å/min), and commercial, in-line equipment is available for comparable prices ($\sim$\$200,000 - \$500,000 depending on the size of the system).

3.2.7 Research on Encapsulation Materials and Methods of Deposition

Our plan for encapsulation materials and methods of deposition has both short- and long-range approaches, both taking advantage of the flat geometry inherent in thin-film modules. Unlike conventional modules which contain thick cells interconnected by metal ribbons, the thin-film module is flat and free of interconnecting wires. In addition, there are no solder joints or junctions of dissimilar metals. Because of these simplicities, substantial quantities of potent materials are not required, and the probability of forming bubbles or voids is considerably reduced.

Our short range work has concentrated on the use of well established encapsulation materials, EVA and Tedlar films, laminated to the back of the module. However, because of the flatness of the module surface, only a thin film (5-10 mils) of EVA is required. This not only reduces material cost but can also simplify the lamination cycle. We have surveyed materials and film extrusion vendors, and have held several meetings with representatives of the DuPont Polymer Products Division[+] to explore the range of existing and future materials. We have established a working relationship with DuPont for both materials development, methods of application, and environmental testing.

[+]E.I. DuPont DeNemous & Co (Inc.), Chestnut Run Laboratories, Polymer Products Dept., Wilmington, DE 19898.

Our short-range work has included laboratory laminations of submodules, and both indoor and outdoor stress testing. The laminations were done initially in a small 13" x 13" laboratory laminator. In June, we received a Spire[++] 240 commercial laminator which has been used in our recent work. Indoor, environmental stress testing is conducted in an environmental temperature/humidity chamber, and in a laboratory-type temperature controlled water bath.

Experiments were conducted to determine the minimum cycle time for laminating sandwiches of 18 gauge/4 gauge EVA/Tedlar. One, two, five and 15 min. cycles were explored. Lamination and curing were separate steps in the 1, 2, and 5 min. cycles . Cure was 15 min. at 150°C. Adherent laminations free of bubbles or voids were obtained in all cases. In water (40°C) soak tests, the samples made with a 1 min. cycle showed evidence of delamination after about 24 hours, while all other samples remained intact during this and other stress tests. For 18 mil EVA, it appears that a 2 min. lamination cycle is sufficient. Thinner EVA might allow an even shorter cycle; however, we cannot obtain thinner films of EVA at present.

We are now fabricating complete active submodules having external electrical connectors. The electrical connectors are Al strips fastened to the Al back contacts of the module by ultrasonic bonding. These submodules are being extensively stress tested in both the indoor and outdoor laboratories.

We are also exploring the concept of using a single or composite film having an adhesive on one side, applied by roll-on or press-on methods. This is similar to the way in which 1½ mil Tedlar films are applied to aluminum siding. It is envisioned that this method could be of extremely high throughput, and is compatible with "in-line" processing concepts. Such films are currently under development at DuPont and will be made available to Solarex in the near future.

[++]Spire Corp., Patriots Park, Bedford, MA.

SECTION 4.0

TASK NO. 3: AMORPHOUS SILICON SOLAR CELLS

4.1 INTRODUCTION

The goal of work performed under this task has been to prepare high efficiency devices, initially in the range of 10%, and to investigate the stability of p-i-n devices toward the ultimate goal of preparing 10% devices which degrade less than 2% in 720 hrs of AM1 exposure.

Toward this goal we have investigated SiC p/i/n structures prepared from silane or disilane, deposited at rates up to 8-9 Å/sec, investigated various means for enhanced optical absorption within the film and explored the effect of impurities on the device performance.

Stability research has been directed at quantifying the degradation rate of these devices, performing measurements of the degradation as a function of exposure time and temperature in order to develop an empirical model of the degradation rate of the devices and establishing the present state of the art for stable devices.

We deal with each of these subjects in the following sections.

4.2 HIGH EFFICIENCY DEVICES

Devices with conversion efficiencies as high as 10.5% have been prepared using a SiC p/i/n structure on tin oxide glass. The parameters for the optimum composition of the p-doped layer were investigated by varying the Si/C ratio and characterizing the resulting doped films from measurements of the dark and light conductivity, activation energy and device performance. The silicon carbide films were prepared from a mixture of silane or disilane, methane and diborane. No advantage was seen from using disilane as a source gas, except of course the higher deposition rate. Disilane deposition rates are a factor of two larger than silane at the same power level. Table 4-1 summarizes the data for several

TABLE 4-1

ELECTRICAL AND OPTICAL DATA FOR $Si_{1-x}C_x$ FILMS DOPED WITH DIBORANE. (ALL CONCENTRATIONS REFER TO GAS PHASE COMPOSITIONS.)

Film Composition	B_2H_6 %	Dark Conductivity $(ohm\text{-}cm)^{-1}$	E_g, (eV)	$T_{substrate}$,(°C)
$Si_{0.8}C_{0.2}$ disilane	.18	3.1×10^{-4}	-	250
$Si_{0.5}C_{0.5}$ disilane	.18	1.4×10^{-5}	2.02	250
$Si_{0.5}C_{0.5}$ disilane	.37	3.5×10^{-4}	1.87	300
$Si_{0.5}C_{0.5}$ disilane	.15	3.1×10^{-5}	1.98	300
$Si_{0.5}C_{0.5}$ disilane	.075	4.2×10^{-6}	2.02	300
$Si_{0.5}C_{0.5}$ silane	.75	1.2×10^{-3}	1.84	300
$Si_{0.5}C_{0.5}$ silane	.18	1×10^{-5}	1.95	300
$Si_{0.5}C_{0.5}$ silane	.075	1×10^{-5}	1.99	300
$Si_{0.5}C_{0.5}$ silane	.18	3×10^{-6}	1.92	250

such films made in a dc discharge. Similar results are obtained for rf discharges if the discharge power densities are similar. Lower temperatures generally result in wider bandgap p-layers owing to the incorporation of a larger percentage of hydrogen; however, much of the excess hydrogen apparently bonds preferentially to boron resulting in a film with a higher resistivity [11]. Although increasing boron concentration in the p-layer gives rise to lower resistivity doped films, which would be expected to increase the built in voltage, devices fabricated with such films show a reduced blue response which cannot be accounted for on the basis of increased optical absorption in the films. Instead we hypothesize that diborane effuses out of the porous film, contaminating the i-layer and degrading the transport properties within that portion of the film adjacent to the p-layer.

Experimentally, the best device performance was obtained with a diborane concentration of 0.18% using a 50% SiH_4, 50% CH_4 discharge atmosphere with a substrate temperature of 250°C. The optimum p-layer thickness was 120Å, calculated from the deposition rate.

The rear contact of the device plays an important role in optimizing the performance since thickness of the i layer is limited by the transport properties of the material. Texturing the substrate increases the effective optical path length, increasing the short circuit current. Three rear contacts have been used in the present study: aluminum, titanium/silver, and ITO/silver. The calculated short circuit currents for the three contacts are given in Table 4-2. It can be seen from this data that small but significant improvements can be obtained from the use of either Ti/Ag or ITO/Ag compared to pure aluminum. Practical problems have been encountered in the use of both the Ti/Ag and ITO/Ag contacts. Ti/Ag contacts frequently give rise to devices which cannot be cured by reverse bias treatment; apparently the local heating which vaporizes the shorted aluminum contact lowers the resistance of the shunt in the case of the Ti/Ag contact. Although the mechanism of the effect has not yet been determined, silver may be diffusing into the amorphous silicon as a result of the high temperature developed locally as in the case of copper.

ITO/Ag contacts are attractive because they should achieve virtually the highest possible rear reflectance when the thickness of the transparent conductor is adjusted to give constructive interference. Towards this end, we have developed

TABLE 4-2

CALCULATED SHORT CIRCUIT CURRENT DENSITIES
FOR THREE REAR CONTACT CONFIGURATIONS

	Reflectance	J_{sc}, AM1
Aluminum	.75	16.9mA/sq cm
Ti/Ag	.90	17.2mA/sq cm
ITO/Ag	1.00	17.5mA/sq cm

a method of depositing high conductivity ITO by sputtering from the oxide source. While the conductivity of the films is high (100 ohms/□ for 600Å film) the resulting devices have low fill factor due to a high rear contact resistance. The reason for the high contact resistance is unclear although some interfacial effect appears likely; work to develop this contact is continuing. Nevertheless, this contact arrangement appears promising; quantum efficiencies as high as 53% at 700 nm have been obtained in devices on textured tin oxide (Fig. 4-1).

High efficiency devices have been fabricated with the structure tin oxide (textured)/p-$Si_{0.5}C_{0.5}$/i-a-Si:H/n^+a-Si:H in which the tin oxide was 7200Å, the p-layer was approximately 100Å thick followed by an undoped region (0.5μm) and a 250Å phosphorus doped layer. The best device had an efficiency of 10.5% with an area of 0.051cm^2; 10.3% was achieved on devices of 0.2cm^2; 9.3% was achieved with 1.2cm^2 area devices. Figure 4-2 gives the I-V characteristic of the 10.5% device. The devices were prepared in a dc discharge without any boron doping in the i layer. For devices made in rf discharges in pure SiH_4, the best efficiency to date is 8.5% with textured tin oxide. For discharge atmospheres of SiH_4 in H_2, the best efficiency is 7% without light trapping.

Photovoltaic parameters of selected cells are listed in Table 4-3. These cells were measured at both Solarex and SERI under the conditions specified in the table.

4.3 IMPURITY EFFECTS

It is clear from a number of recent publications that impurities can have significant effects on both carrier transport properties and stability of devices [12, 13, 14]. In single chamber deposition systems such as used in these experiments, impurities can arise from two sources: first, outgassing of the chamber walls and second, from trace quantities of dopants remaining from previous depositions of the n or p layers.

Boron dopant has been associated with a improvement in both device efficiency and stability [15]. In our experiments, the effect of boron addition was explored by adding trace quantities, up to 10ppm, to silane during the

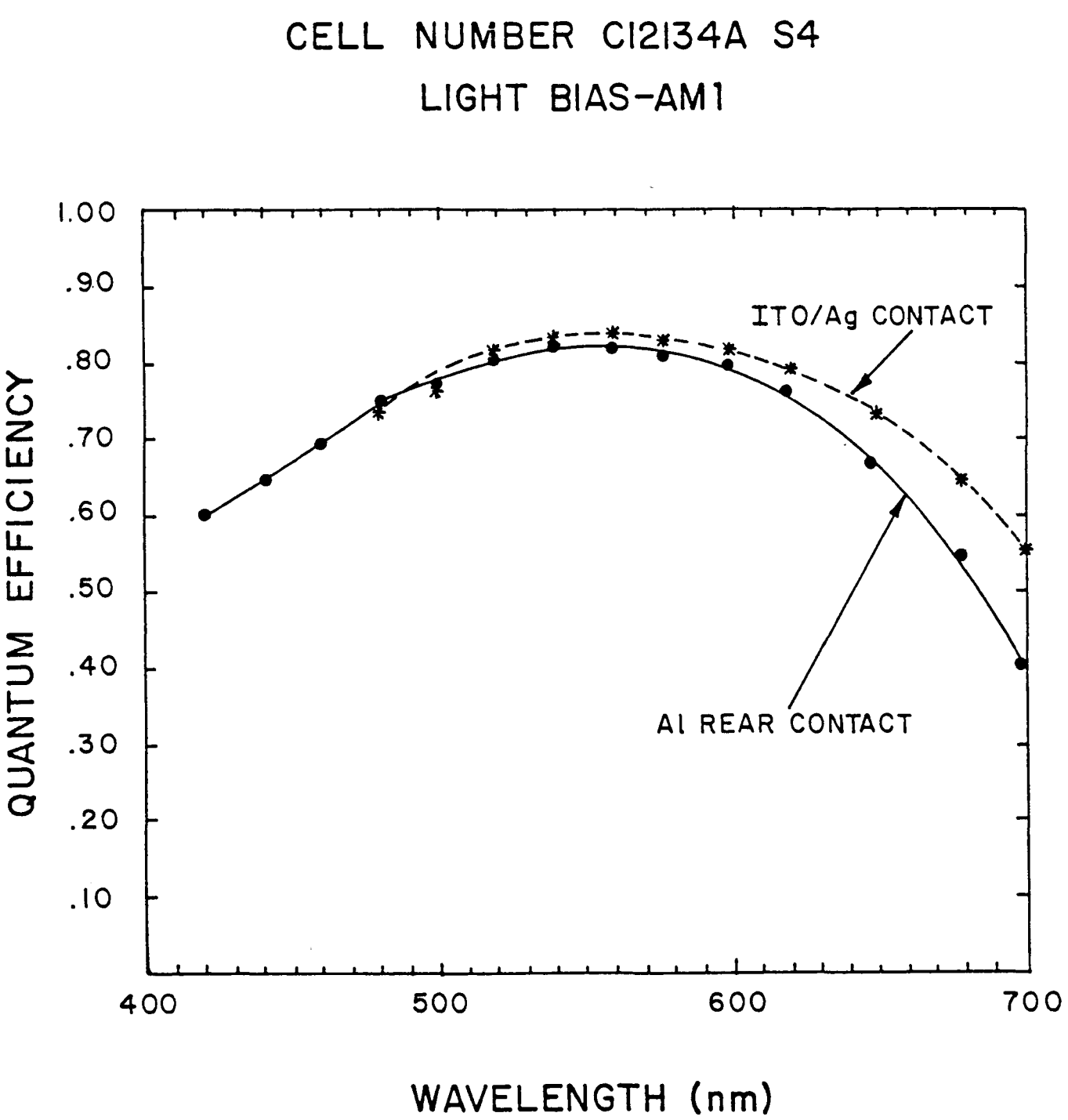

FIGURE 4-1. SPECTRAL RESPONSE CURVE OF A P-I-N SOLAR CELL WITH AN ITO/Ag BACK CONTACT.

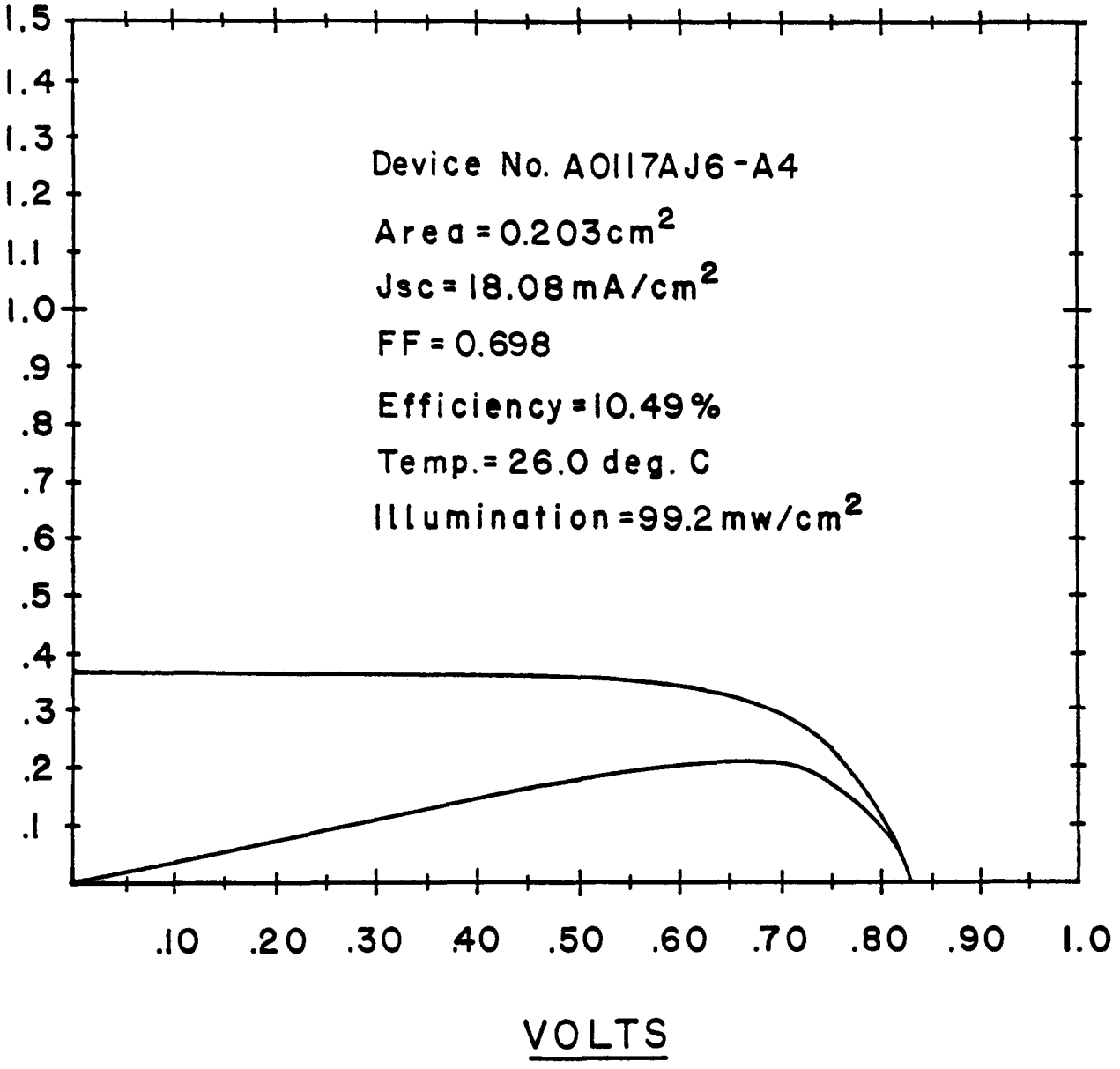

FIGURE 4-2. CURRENT-VOLTAGE CHARACTERISTIC OF AN a-Si:H P-I-N SOLAR CELL.

TABLE 4-3

PHOTOVOLTAIC PARAMETERS OF SELECTED CELLS

Sample No.	Date Meas.	Time Meas.	Light Source	Temp Cell (Ambient)	Location	J_{sc} mA/cm^2	Voc mV	FF	%	Area cm^2	Comment
A1221AJ1BA1	12/27/84		Oriel	27°	Solarex	15.95	831	.683	9.05	0.203	
A1221AJ1BA1	1/03/85	2:22p	SIM	28°	SERI Lab	14.90	854	.669	8.5	0.207	
A1221AJ1BA1	1/03/85	3:17p	SIM	28°	SERI Lab	14.87	847	.641	8.1	0.207	Looks shunted
A1221AJ1BA1	1/04/85	1:39p	Sun	(17.5°)	SERI Outdoor Lab	15.67	837	.634	8.3	0.203	(915mW/cm^2)
A1221AJ1BA1	1/08/85		Oriel	27.4°	Solarex	15.53	830	.639	8.2	0.203	
A1221AJ16A3	12/27/84		Oriel	27.1	Solarex	16.34	844	.712	9.82	0.203	
A1221AJ16A3	1/03/85	2:35p	SIM	28°	SERI Lab	14.91	858	.704	9.0	0.210	
A1221AJ16A3	1/03/85	2:38p	SIM	28°	SERI Lab	14.89	856	.699	8.9	0.210	
A1221AJ16A3	1/04/85	1:55p	Sun	(16.3°)	SERI Outdoor Lab+	15.71	867	.678	9.2	0.203	
A1221AJ16A3	1/04/85	1:53p	Sun	(16.6°)	SERI Outdoor Lab	15.76	(867)	.710	9.70	0.203	V_{oc} error/see curve
A1221AJ16A3	1/08/85		Oriel	27.3°	Solarex	15.94	846	.687	9.26	0.203	
A1221J16W1	12/27/84		Oriel	27°	Solarex	15.58	841	.705	9.25	1.29	
A1221J16W1	1/03/85	3:10p	SIM	28°	SERI Lab	14.89	862	.694	8.9	1.298	
A1221J16W1	1/03/85	3:12p	SIM	28°	SERI Lab	14.88	857	.692	8.8	1.298	
A1221J16W1	1/04/85	1:58p	Sun	(16.9°)	SERI Outdoor Lab	15.23	850	.674	8.8	1.29	
A1221J16W1	1/04/85	2:00p	Sun	(16.3°)	SERI Outdoor Lab	15.17	857	.672	8.7	1.29	
A1221J16W1	1/08/85		Oriel	28°	Solarex	15.4	831	.679	8.7	1.29	

+Note: Insolation measurement uncertainity ±5%

deposition of the i-layer. Somewhat surprisingly, the effect of boron doping was found to depend on the concentration of background impurities. In well outgassed (24 hrs) systems, any addition of boron resulted in a decrease in device efficiency due a decrease in both open circuit voltage and fill factor.

In this case, boron may add defect states to the i-region and increase recombination. In contrast, poorly outgassed (2.5 hrs) systems which contain high partial pressures of water vapor, CO and CO_2 benefit from boron doping. Those devices show a well defined maximum efficiency when 3ppm boron is added to the i-layer. The improvement in device performance results from an increase in fill factor, and fill factors as high as 72% have been obtained in this manner. Figures 4-3 and 4-4 give details of the experimentally observed dependence on boron concentration for the two cases.

In single chamber systems, device performance may degrade due to cross contamination of the i-layer from dopants introduced to form the p-layer or n-layer. To test the significance of this effect devices were deposited consecutively in a single chamber load-lock system. Since the chamber was not well outgassed prior to the first device, the carrier collection length and performance were low. The flat band potential measured at 700nm, 500nm and 400nm indicated that the electric field in the device was larger at the rear contact (Figure 4-5). After eight deposition runs the flat band was nearly the same at all wavelengths and the collection length improved, although the blue response remained relatively low. After fourteen runs the field appeared highest at the p/i interface and the built in voltage was highest at 400nm. The latter result suggests that phosphorus contamination of the i-region may be significant in that film. SIMS analysis is being performed at this writing in order for us to understand the origin of the effects.

4.4 STABILITY STUDIES

Amorphous silicon solar cells degrade under prolonged illumination. Hence, studies of the long term stability of these cells are critical to developing an understanding of the degradation mechanisms. In the present work we have studied the rate of degradation of the conversion efficiency of p-i-n solar cells with time. This study includes the effect of the i-layer thicknesses, the impurity content, and the temperature on the stability of these cells.

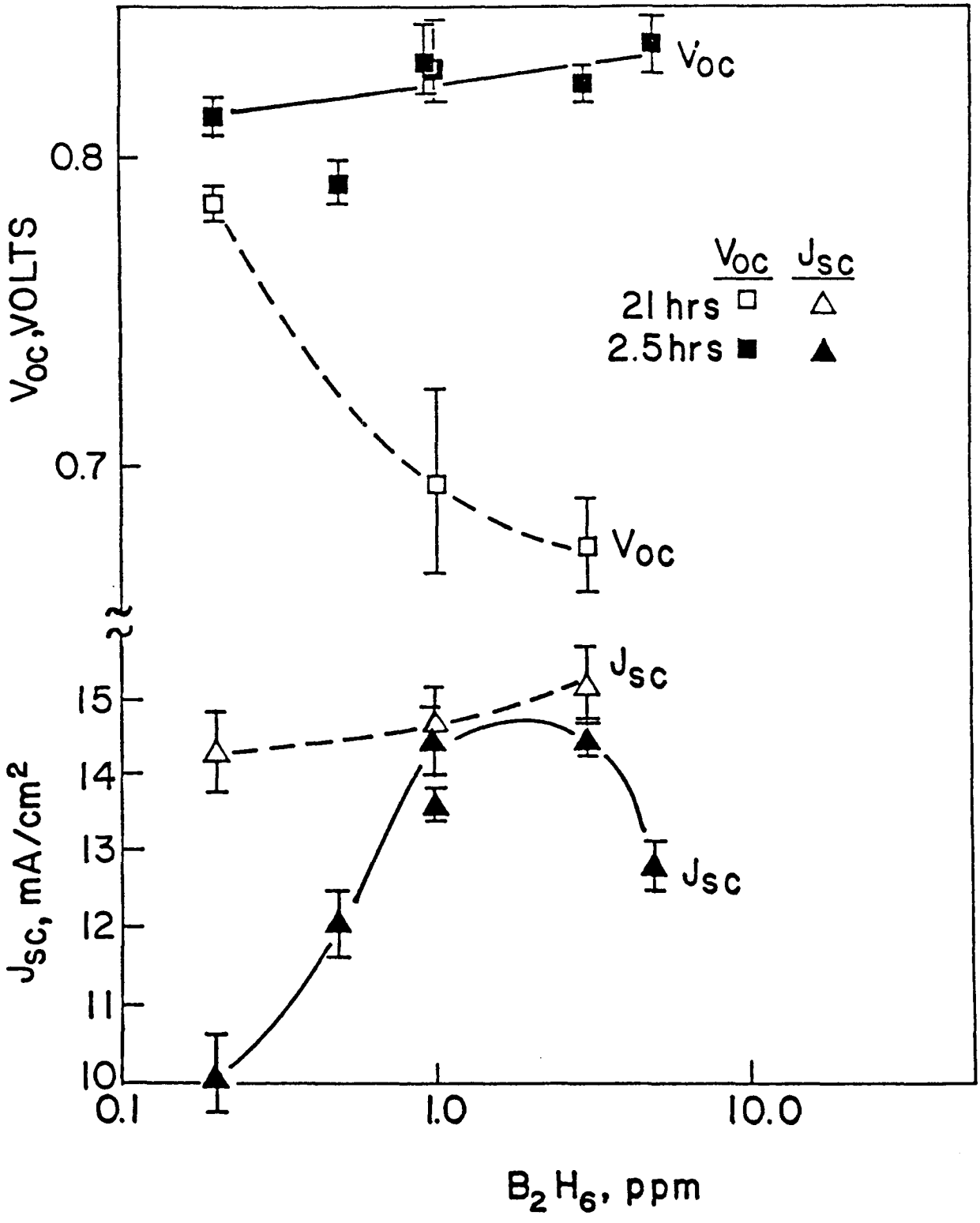

FIGURE 4-3. OPEN-CIRCUIT VOLTAGE AND SHORT-CIRCUIT DENSITY AS A FUNCTION OF DIBORANE IN THE I-LAYER.

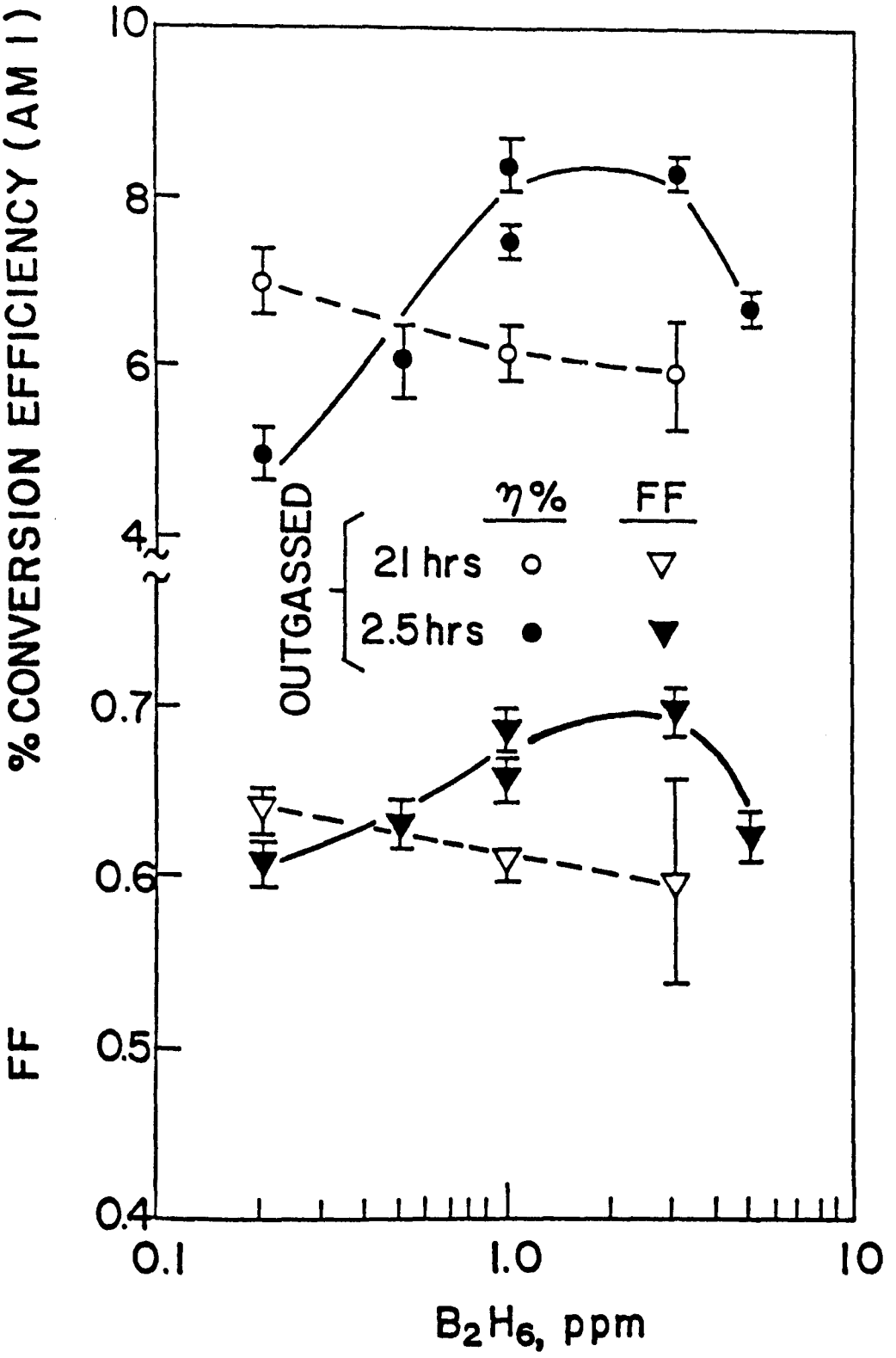

FIGURE 4-4. CONVERSION EFFICIENCY AND FILL FACTOR AS A FUNCTION OF DIBORANE IN THE I-LAYER.

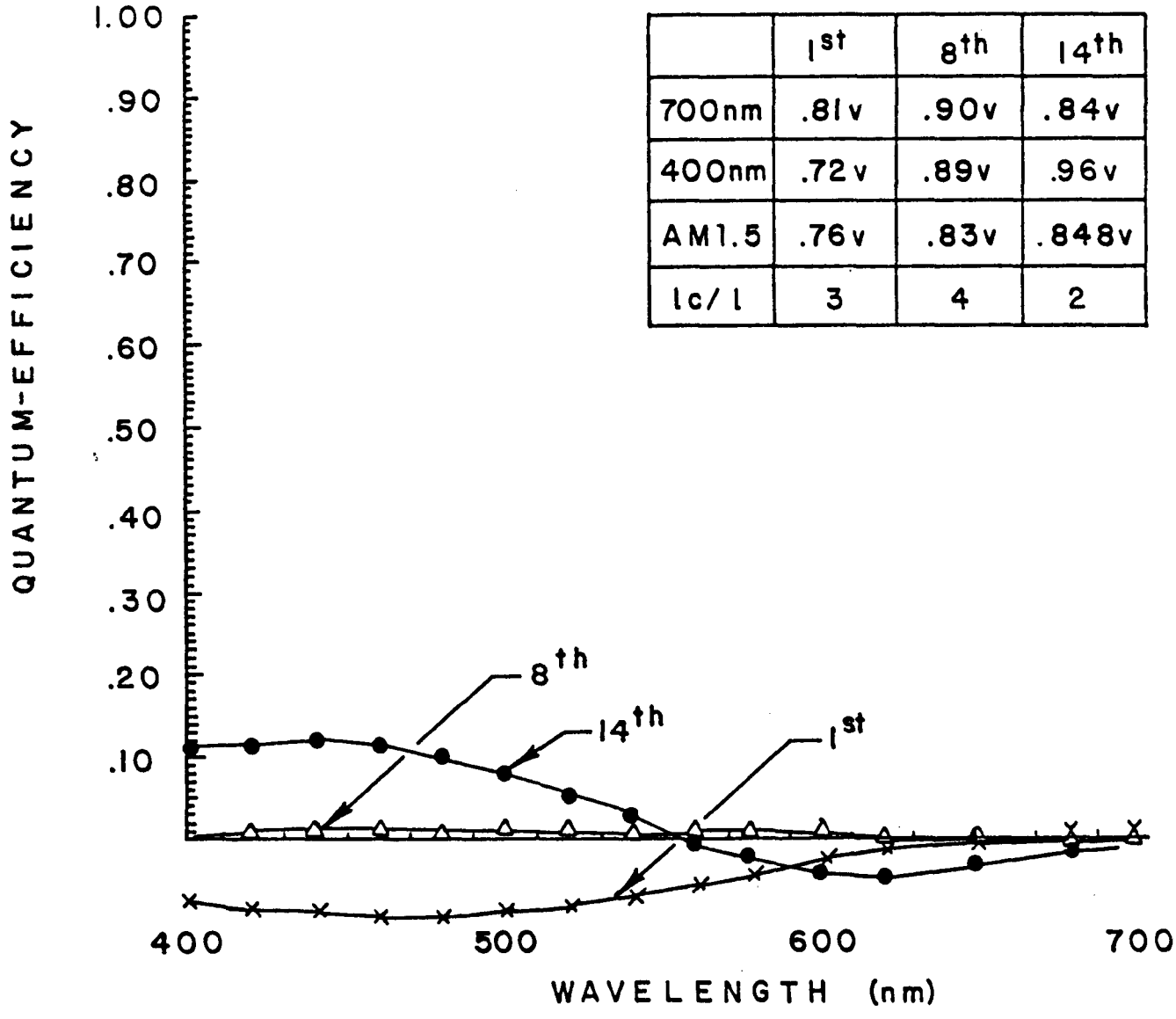

	1st	8th	14th
700nm	.81v	.90v	.84v
400nm	.72v	.89v	.96v
AM1.5	.76v	.83v	.848v
lc/l	3	4	2

FIGURE 4-5. SPECTRAL RESPONSE CURVES MEASURED AT A FLAT BAND POTENTIAL FOR THE 1st, 8th, AND 14th RUNS IN A LOAD-LOCK SYSTEM.

4.4.1 Experimental Conditions

All the solar cells used for this study had initial conversion efficiencies (under simulated AM1 conditions) in excess of 7% (area $\simeq$ 1 cm^2) and had the following cell structure: glass/SnO_2:F/p-i-n/Al or Ti - Ag.

The cells were light soaked either under sodium vapor lamps (GE #LU400) or under ELH lamps. The intensity of illumination (AM1) was calibrated by using a "standard silicon cell" with an appropriate filter. The temperature was controlled within ± 4 °C either by fans or by using thermoelectric temperature controlled stages. The I-V characteristics of these cells under AM1 illumination was periodically measured by using an Oriel solar simulator.

4.4.2 Results

Figure 4-6 shows the degradation of efficiency with time for cells with two different i-layer thicknesses. These cells were light soaked under AM1 illumination at 308 ± 4 °K. Each data point is an average of two cells. The upper curve is for cells in which the i-layer was 2780Å thick and the lower curve is for cells with 5800 Å thick i-layer. After 750 hours of continuous illumination the thicker i-layer cells degrade to about 50% of their initial value. In the same time period, the thinner i-layer cells degrade to about 65% of their initial value. The thinner i-layer cells degrade less because the electric field in these cells is higher than that of the thicker cells. The higher electric fields reduce the effects of light-induced recombination of carriers. This has important consequences, particularly for 2 or 3 stacked junction solar cells where the i-layers of the individual cells are thinner than the i-layers of conventional single junction solar cells. In a single junction p-i-n solar cell, reduction of the i-layer thickness results in lower values of the short circuit current and consequently lower values of conversion efficiencies. Nevertheless, we have fabricated cells with i-layer thicknesses of only 2780Å with conversion efficiencies in excess of 7%. These cells had short circuit current densities in the range of 14.3 to 14.8 mA/cm^2. We feel that by proper optical confinement, cells with this i-layer thickness can result in conversion efficiencies in the range of 8.5 to 9%.

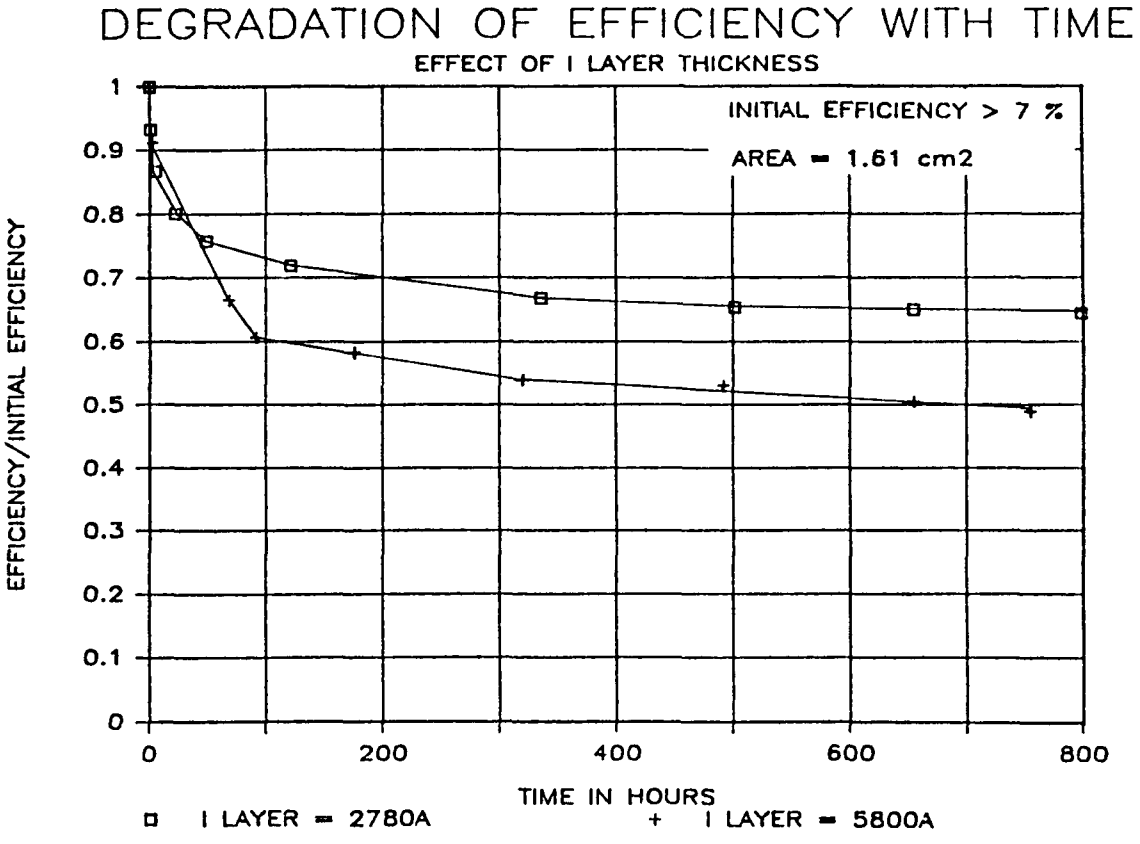

FIGURE 4-6. RELATIVE CONVERSION EFFICIENCY AS A FUCNTION OF EXPOSURE TO AM1 ILLUMINATION FOR P-I-N CELLS WITH DIFFERENT I-LAYER THICKNESSES.

Figure 4-7 shows the degradation of efficiency with time under AM1 illumination at 308 ± 4 °K for cells deposited under different conditions. Both the curves are for 5800Å thick i-layer cells. The upper curve is for cells deposited after sufficient "bakeout" of the deposition system. Consequently, the impurity content in the device, particularly the oxygen content, is on the order of 10^{19} cm^{-3}. The lower curve is for cells deposited after a short pumpdown. In these cells, it is expected that the oxygen content is on the order of 10^{20} cm^{-3} or even higher. After 750 hours of continuous illumination the cells with higher impurity content degrade to about 35% of their initial value; whereas in the same time period, the cells with lower impurity content degrade to 50% of their initial value. Clearly, oxygen and other impurities incorporated from the deposition system have a detrimental effect on the stability of these cells.

Figure 4-8 shows the stability of the same cells as in Figure 4-7 but were light soaked at two different temperatures. The upper curve is for cells light soaked at 323 ± 4 °K and the lower curve is for cells light soaked at 308 ± 4 °K. After about 800 hours of continuous illumination, the cells kept at 323 °K degrade to approximately 50% of their initial efficiency whereas in the same time period, cells kept at 308 °K degrade to 35% of their initial efficiency. The effect of light induced degradation in amorphous silicon solar cells can be viewed as a combination of two competing processes; (i) the forward rate of creation of defects, and (ii) the reverse rate of self-annealing of defects. The light-induced defects that are created can act as traps or recombination centers. This forward rate would be dependent on the dose of illumination. On the other hand, the self-annealing of defects is an activated process, and hence the rate would be temperature dependent. A study of degradation as a function of light intensity and temperature should lead to a better understanding of the kinetics of formation and annealing of light-induced defects. We have initiated a detailed study of intensity-temperature-time effects on the stability of our cells. The initial results indicate that reciprocity holds, i.e., the degradation of efficiency depends only on the product of light intensity and exposure time, in contrast to recently published results [16].

FIGURE 4-7. RELATIVE CONVERSION EFFICIENCY AS A FUNCTION OF EXPOSURE TO AM1 ILLUMINATION FOR P-I-N CELLS WITH DIFFERENT BAKEOUT CONDITIONS.

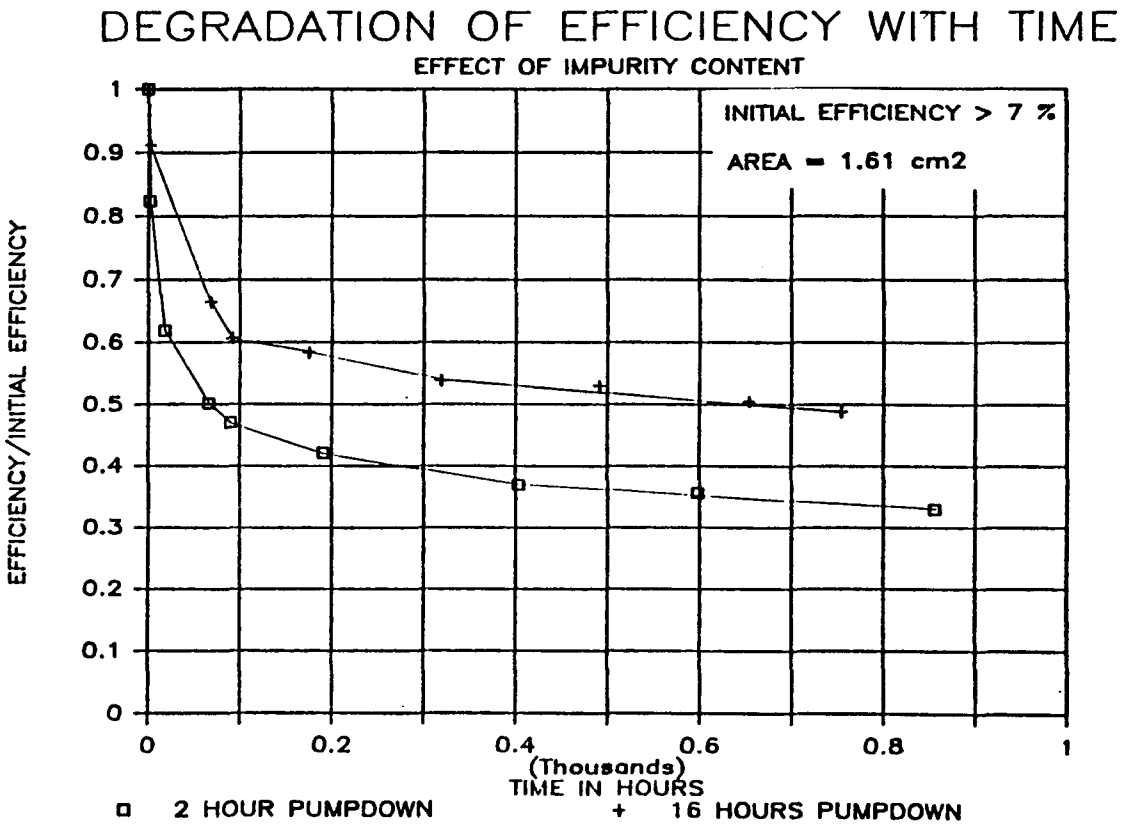

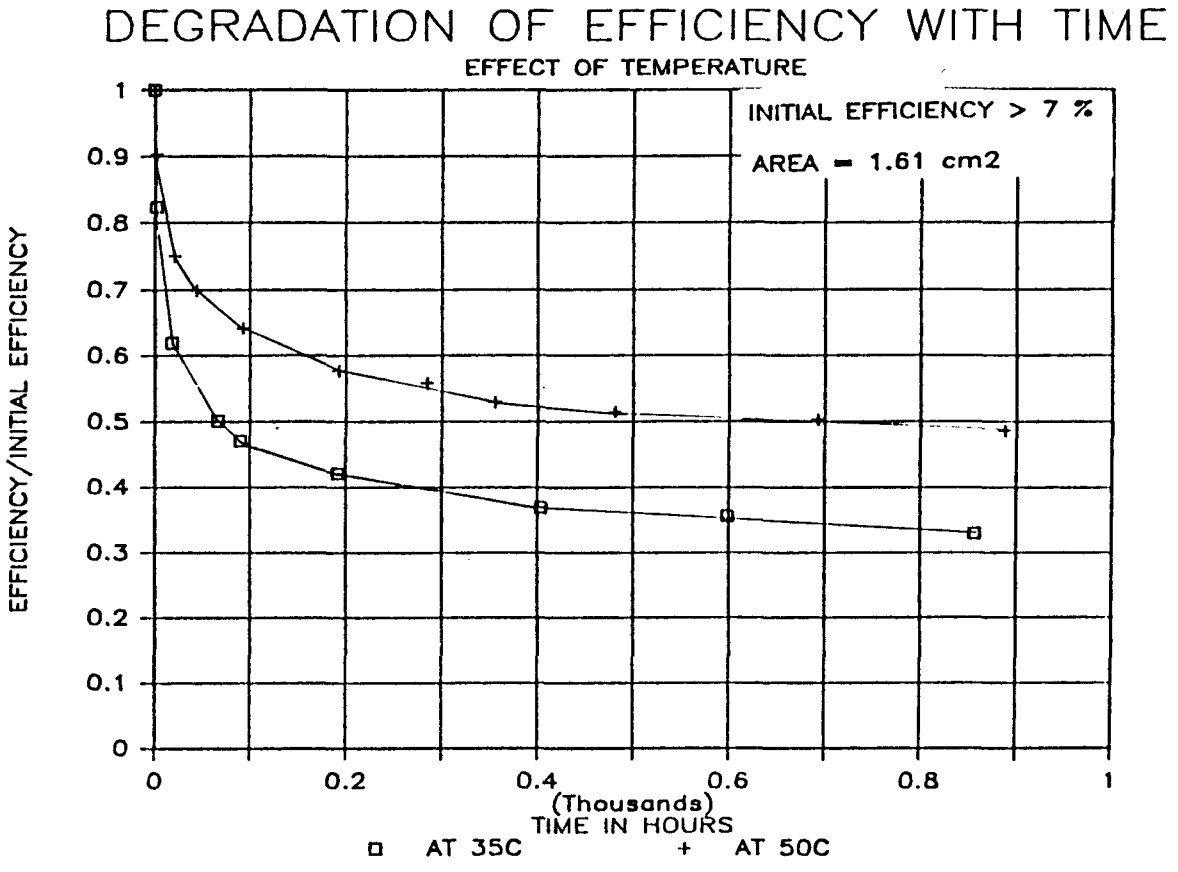

FIGURE 4-8. RELATIVE CONVERSION EFFICIENCY AS A FUNCTION OF EXPOSURE TO AM1 ILLUMINATION FOR P-I-N CELLS THAT WERE LIGHT SOAKED AT DIFFERENT TEMPERATURES.

SECTION 5.0

TASK NO. 4: MONOLITHIC, INTRA-CONNECTED CELLS/SUBMODULE RESEARCH

5.1 BASELINE SUBMODULE DESIGN

Figures 5-1 and 5-2 shows the baseline design for a submodule with overall glass dimensions of 12" x 13". The submodule consists of 12 parallel strings, each containing 35 series-connected cells. Assuming a current density of 14mA/cm^2, and 0.8 volt/diode the expected, electrical output characteristics are as shown in the lower inset of Fig. 5-1. In calculating these values, a moderate fill-factor range of 0.53 to 0.59 was assumed. The design results in several area losses such as borders, metal separations, bus-bars, and tolerances for screen printing. These losses are listed in Table 5-1 below. The initial separation and tolerance losses (total 6.8%) could be almost completely eliminated if the laser patterning of metal as described in Section 5.4 is successfully developed. This would result in a 90.2% active area for this submodule design.

Table 5-1

AREA LOSSES FOR SUBMODULE DESIGN OF FIG. 5-1

Loss Cause	Area Lost	%
Border loss	46.7cm^2	4.6
Parallel string metal opening (0.025")	19.6cm^2	2.0
Metal separation (0.015")	43.0cm^2	4.3
Bus bars (2 each)	32.8cm^2	3.3
Tolerance (0.010")	25.0cm^2	2.5
Net Loss	167.1cm^2	16.6%

Net Active Area = 1006.4 - 167.1 = 839.3cm^2 or 83.4%

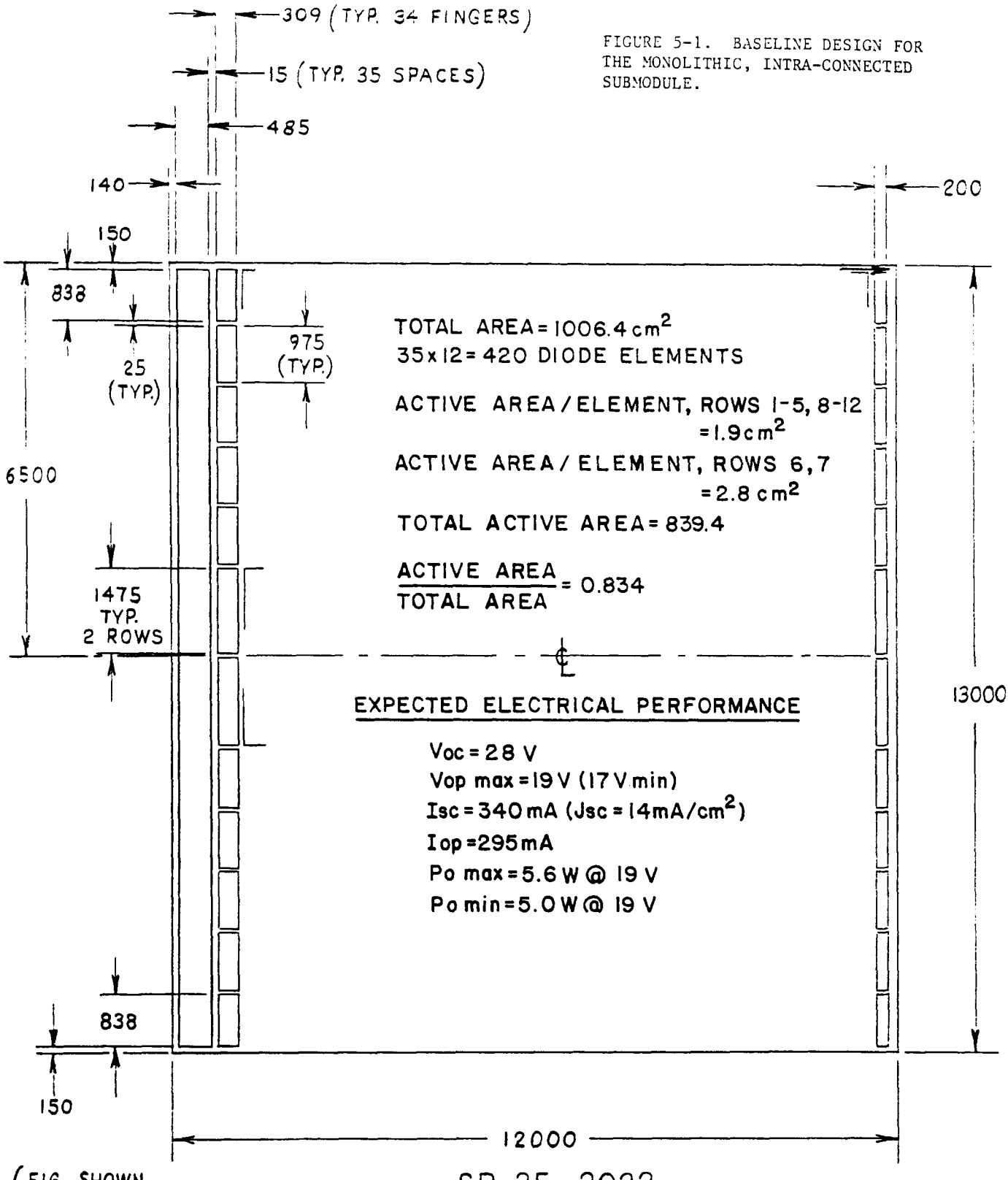

FIGURE 5-1. BASELINE DESIGN FOR THE MONOLITHIC, INTRA-CONNECTED SUBMODULE.

(FIG. SHOWN 1/2 ACTUAL SIZE)

SB-35-3033

POWER MODULE METAL PATTERN

12" x 13" SUBSTRATE (0.125" SODA-LIME GLASS)

FIGURE 5-2. BASELINE DESIGN FOR THE LASER PATTERNING OF THE TIN OXIDE AND THE a-Ai:H OF THE MONOLITHIC, INTRA-CONNECTED SUBMODULE.

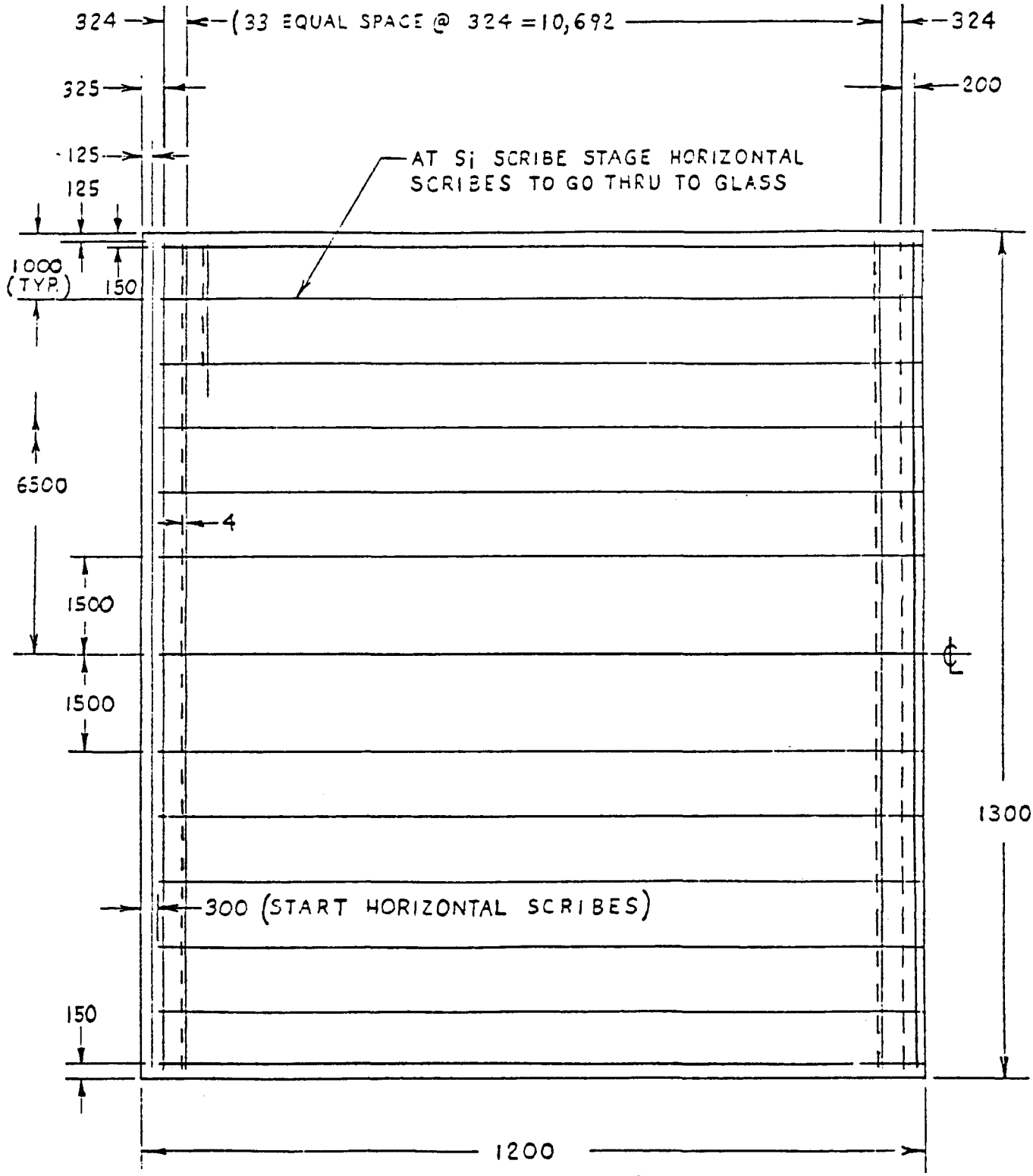

SB-35-3033

POWER MODULE METAL PATTERN

12"x 13" SUBSTRATE (0.125" SODA-LIME GLASS)

The design has two features intended to ease the attainment of good performance. Most individual diodes have small area (1.9cm^2), and the 12 parallel strings can be individually measured before they are interconnected by an aluminum ribbon bus. Thus, in principle, each of the 420 diodes could be treated separately, and any of the 12 rows whose performance is deemed unsatisfactory could be omitted from the interconnection. Leaving out a row would of course reduce the net current by 1/12, but the remaining strings would not be "load-down" by a low voltage row. We have used both of these features as is described below.

5.2 STATUS OF DEPOSITIONS ON LARGE AREAS

As mentioned in Section 3.2.2, we have succeeded in depositing tin oxide with reasonable uniformity over all areas of 400cm^2 using a laboratory CVD belt furnace. The sheet resistivity averages about 25 $\Omega/\square$ in this case. The Watkins-Johnson belt furnace has been tested, and shows the capability of depositing tin oxide uniformly over areas $\sim$ 1000cm^2 with $R_\square \lesssim 10\ \Omega/\square$.

We have deposited uniform coatings of a-Si:H over areas of 1000cm^2 using a Solarex multi-chamber deposition system (see Section 6.2). Aluminum has also been deposited over areas of 1000cm^2 using an S-gun metallization system and an in-line DC magnetron system.

5.3 DEVICE CHARACTERIZATION

We presently have the capability to measure I-V characteristics for submodules up to 1000cm^2 in area. We have ordered an illuminator that can handle modules up to 24" x 24". An outdoor test facility has recently been constructed and is operational. The conversion efficiencies of submodules are measured outdoors using both pyroheliometers and calibrated crystalline silicon cells (supplied by NASA) to measure the solar insolation.

We are presently using an infrared camera to determine the uniformity of submodules. Recent results indicate that the uniformity and quality of laser-scribed interconnect regions can be analyzed by examining the submodule in forward bias with the infrared camera. In reverse bias, the camera can detect localized shorts due to pinholes or localized shunts caused by pinholes or debris in the doped layers.

Several modules as described above were made during the latter part of Phase I of this contract. The process sequence listed in Table 5-2 was used, and typical and best results obtained to date are shown in Fig. 5-3 and 5-4. The areas of the submodules as shown in the data insets are active areas for the rows which were selected for interconnection. For the module in Fig. 5-4, nine of the twelve rows were connected, while ten rows were used in that of Fig. 5-3. The current/voltage parameters obtained are in reasonable agreement with the projections of Fig. 5-1 when the current loss due to the omitted rows is taken into account. The active area efficiency of 6.07% is quite encouraging and is in good agreement with small area cells made in the same deposition equipment.

5.4 LASER SCRIBING SYSTEMS

As part of the cost sharing part of this contract, the Solarex Thin Film Division has directed Lasermetrics Inc. of Englewood, NJ, to build a state-of-the-art laser scribing system to provide patterning of TCO, a-Si:H, and metal films used to fabricate amorphous silicon solar cells. The date of delivery for this system is March 1985. Until this system is delivered, the Solarex Thin Film Division is using one of its presently operating in-house laser scribing systems to pattern TCO, a-Si:H, and metal thin films.

The assembly of the above laser system by Lasermetrics is proceeding on schedule Each of the individual subsystems are discussed briefly.

Part I - Nd:YAG Laser System

The Nd:YAG laser system is a Lasermetrics Model 9560QT capable of delivering up to 14 watts TEM_{oo} and 40 watts Multimode at 1.06 microns. The Rep-Rate is continuously variable from 1 to 50 KHz. The pulse widths will range approximately between 120 and 500 nanoseconds depending on laser mode and Q-switch repetition rate.

TABLE 5-2

PROCESS SEQUENCE

1. Select CTO/glass ($R_{\square} \lesssim 10\ \Omega/\square$, 0.125" thick)+
2. Clean
3. Laser Scribe CTO pattern (see Fig. 5-2)
4. Clean
5. Deposit a-Si ("in-line" system)
6. Laser scribe a-Si and horizontal separations (see Fig. 5-2)
7. Metallize - 4000Å of Al (sputtered)
8. Print resist ink in pattern of Fig. 5-1/cure
9. Etch Al
10. Strip ink
11. Clean & dry
12. Test diodes and rows
13. Ribbon bond bus-bars
14. Test submodule
15. Laminate

+ Purchased from Cherry Display Products, El Paso, Texas

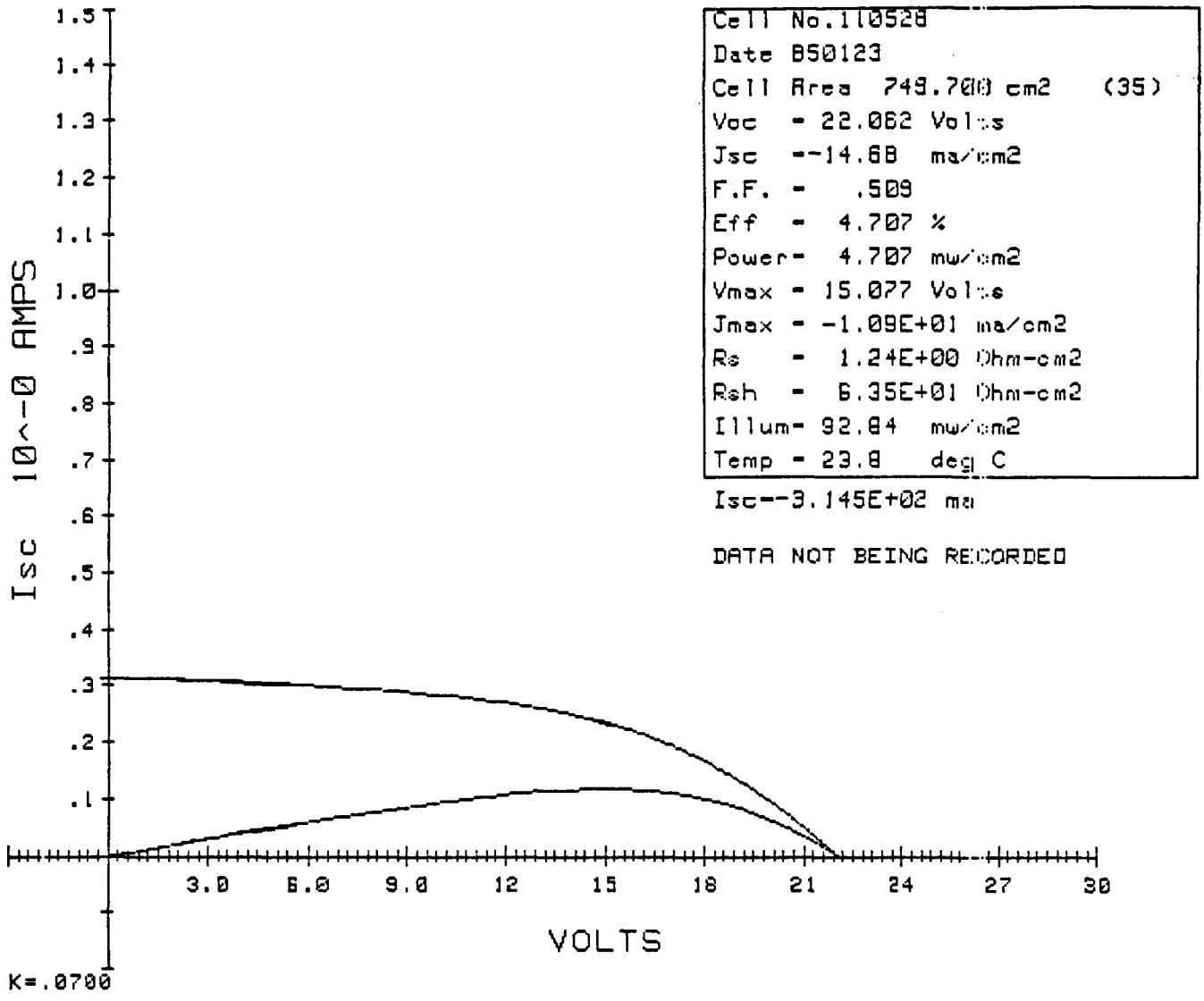

FIGURE 5-3. CURRENT-VOLTAGE CHARACTERISTIC OF A SUBMODULE WITH AN ACTIVE AREA OF 749.7cm^2.

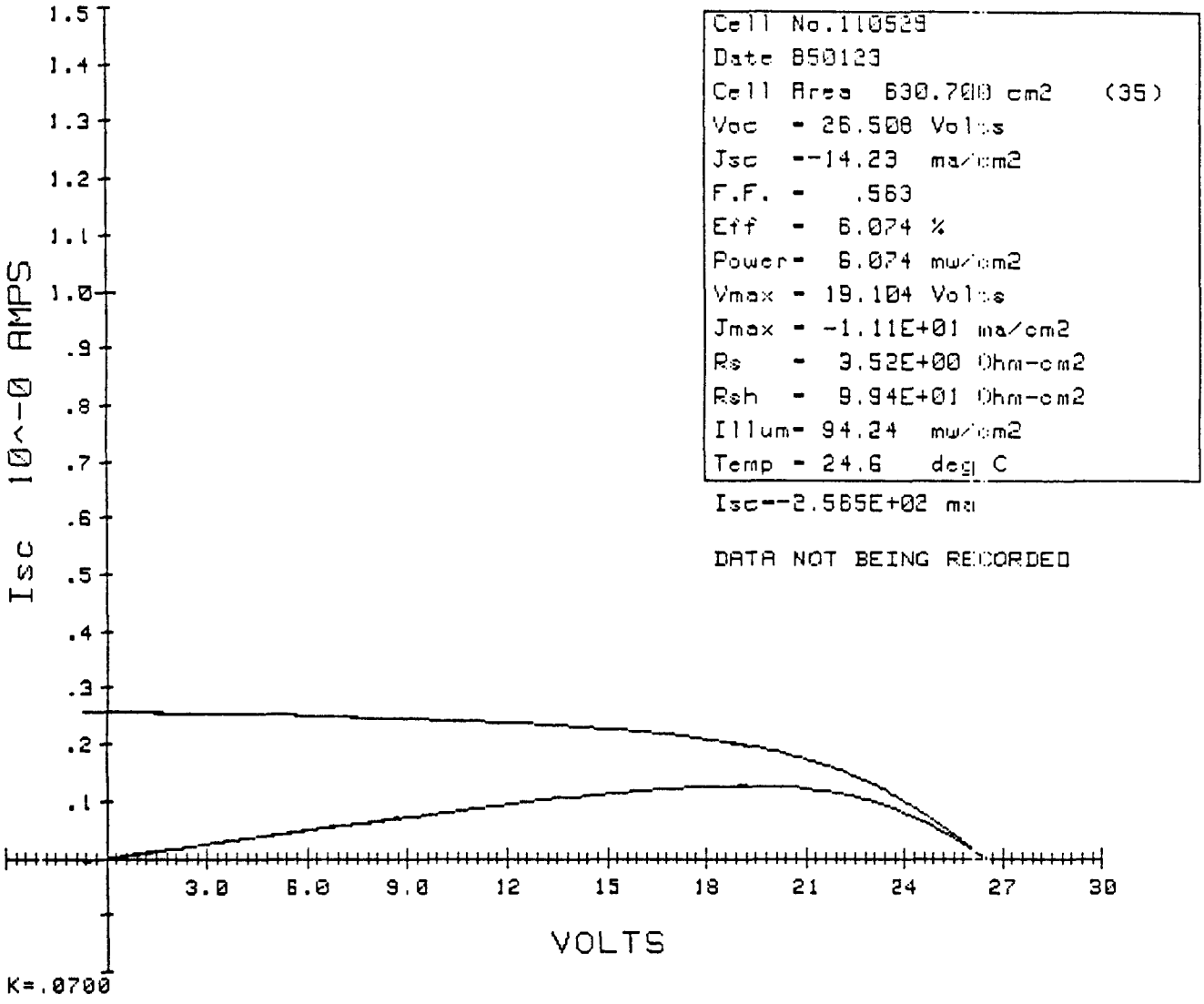

FIGURE 5-4. CURRENT-VOLTAGE CHARACTERISTIC OF A SUBMODULE WITH AN ACTIVE AREA OF 630.7cm^2.

Part II - X-Y Table

1. Table travel 30" x 30", Anorad 14-30.
2. 10"/second rate of translation.
3. Vacuum holder flat 8-20 mils over a linear distance of 12". Two substrate templates are provided 12" x 13" and 12" x 24".
4. The table is capable of less than 1 mil increments to enable parallel scribes within 1 mil.
5. A vacuum system for debris removal while scribing will be provided.
6. The X-Y table has the ability to produce a series of parallel scribes having a 1 mil width separated by distances of 1 mil or less to 0.500". The ability to alter this pattern is part of the programming capability of the table system. It should be noted that 1 mil scribe lines are achievable only in the TEM_{oo} mode. It should also be noted that auto focusing may cause a variation in scribed line kerf width.

Part III - Automatic Focusing System

An Automatic Focusing System is provided with the system. The ability of the system to maintain focus and produce a 1 mil scribe at table speeds in excess of 2" per second may not be feasible. However, experimentation with the Auto-Focus in conjunction with the design of the focusing optics may achieve the required results. Automatic Focusing will be provided on a best effort basis and will be provided for a single beam system.

Part IV - Automatic Alignment and Tracking System

Auto-align is accomplished by the recognition of a predetermined reference, i.e., substrate corners, Fiducial marks or a previously scribed line. Lasermetrics believes the accuracy of the X-Y table selected eliminates the necessity for a tracking system. Table specifications are as follows:

Flatness ± .00005"/" not to exceed ± .0005"/12" of travel
Accuracy, ± .0001"/" of travel not to exceed .0005"/12" of travel
Repeatability, ± .00005 bi-directional
Orthogonality, ± .00005"/" not to exceed ± .0005"/20" of travel

This is a closed loop system utilizing optical encoders. The accuracy of the table is independent of the lead screws.

Part V - Multiple Beam Provision

A provision to deliver four (4) beams simultaneously to the substrate spaced 3 inches apart can be provided. At 1.06μm each beam will deliver approximately 3.00 watts TEM_{oo}. This option quadruples the thruput of the system. Lasermetrics does not believe a system with 50 parallel beams is feasible at this time with spacings of .2 to .250". Auto-focus will not be assembled with the multiple beam system.

Part VI - Computer Control System

Lasermetrics has selected the Anomatic II Programmable CNC Positioning Controller. The flexibility and wide industry acceptance of this Controller make it an ideal choice. A software program to produce parallel scribes is included. Other features are: Mini-floppy disk, 16 input-output M functions, R532 interface and CRT terminal.

SECTION 6.0

TASK NO. 5: MULTI-CHAMBER DEPOSITION SYSTEM

6.1 CONCEPTUAL DESIGN

The conceptual design for an in-line amorphous silicon deposition system was completed during the first six months of the contract. The design features of this system are shown in Figure 6-1, and the deposition conditions selected for operation are listed in Table 6-1.

6.2 SOLAREX MULTI CHAMBER SYSTEM

A multi-chamber in-line system capable of producing amorphous silicon on 1000 cm^2 substrates has been producing both individual layers and operating devices.

Diffusion lengths greater than 0.5 μm have been measured by the surface photovoltage technique in intrinsic layers deposited in the in-line system. Doped layers made in this system show electronic and optical properties similar to those films made in single chamber systems. Boron doped layers have been produced with resistivities of $\sim 10^4$ Ω-cm and carbon containing layers have been produced with a resistivity of $\sim 10^6$ Ω-cm and a bandgap of about 2.0 eV. Phosphorus doped layers have been grown with resistivities in the 10^3 Ω -cm range and bandgaps of about 1.7 eV.

SIMS analysis of the intrinsic layers deposited simultaneously with doped layers indicate boron levels below 10^{17} per cubic centimeter indicating that minimal cross-contamination of dopants is occurring in the system.

Several improvements in the system have been completed during the term of the contract. Temperature control of the substrate heaters has been changed to reduce variations caused by changing atmosphere in the vacuum chambers. The transport of the substrates through the chambers was made more reliable by replacing high temperature bearings with bushings in locations such that the deposition products and heat would cause less problems and improve reliability. The gas introduction system has been changed to reduce the localized high pressure areas causing powder deposits. Initial problems making ohmic contact

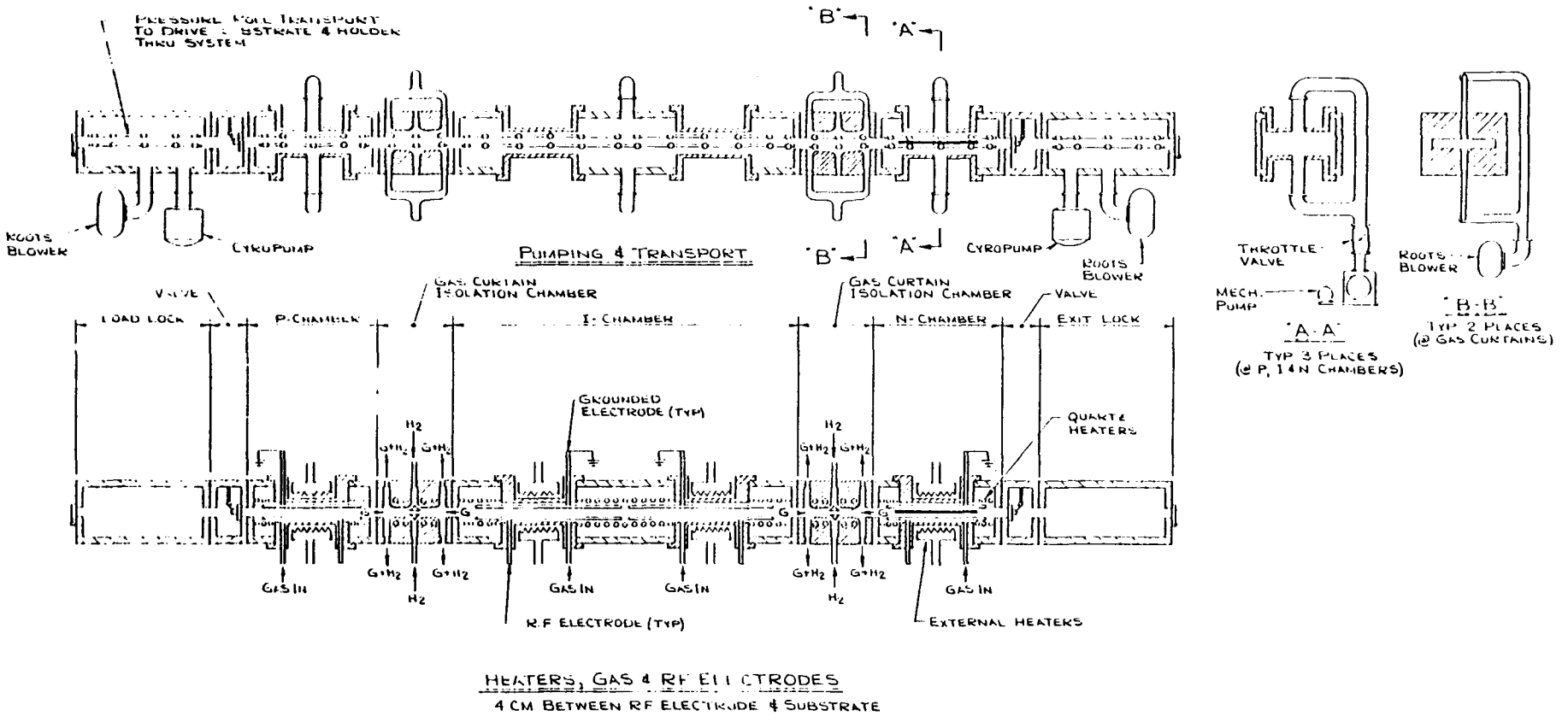

HEATERS, GAS & RF ELECTRODES

4 CM BETWEEN RF ELECTRODE & SUBSTRATE

R.F. MULTI-CHAMBER IN LINE
a-Si DEPOSITION SYSTEM

SOLAREX

D

FIGURE 6-1. A CONCEPTUAL DESIGN FOR A MULTI-CHAMBER DEPOSITION SYSTEM.

TABLE 6-1

DEPOSITION PARAMETERS FOR MULTI-CHAMBER IN-LINE SYSTEM

I-LAYER

Substrate Temperature: 250 - 350°C

Pressure: 0.5 - 2.0 Torr

10 - 50% SiH_4 in H_2

5 - 10% Si_2H_6 in He

P-LAYER

T_s: 250 - 300°C

50 - 70% CH_4 in SiH_4

0.1 - 0.5% B_2H_6 in SiH_4

Hydrogen Dilution

0.1 - 0.3 Watts/cm^2

N-LAYER

T_s: 200 - 300°C

0.5% SiH_4 in H_2

1% PH_3 in H_2

0.5 - 1.0 Watts/cm^2

to the n-layer were thought to be related to exposing the cells to air at elevated temperatures. An extended inert gas cooling chamber was added to the vacuum system to allow slow cooling in an inert atmosphere without adversely affecting system throughput.

Electrical performance on small area devices has surpassed six percent efficiency at AM1. Reproducibility from cell-to-cell is excellent. Efficiencies of about 6% have been obtained on active areas over 600 cm^2.

6.3 MODELING

Model equations using mass balances to describe the flow conditions in a plasma reactor have been developed at the Institute of Energy Conversion under Subcontract STF-2. The modeling simulates the conditions under which a film forms by surface reaction at a heated substrate under various temperature and flow conditions. The effort has centered on developing model equations for analyzing the plasma deposition reactor developed under the conceptual design part of Task 5.

Two simple reaction paths to form a silicon film in the parallel plate reactor have been considered:

1. $SiH_4(g) \xrightarrow{k_s} 2H_2(g) + Si(s)$

and

2. $SiH_4(g) \xrightarrow{k_g} A^*$

   where $A^* \xrightarrow{k_s} 2H_2(g) + Si(s)$

The result of using these reaction paths are equations describing the growth rate and the silane effluent as a function of measurable system parameters. The growth rate for a well mixed reactor can be described as follows:

$$\text{Growth Rate} = \frac{MW_{si}}{\rho_{film}} (k_1 V Y_{SiH_4}) \frac{P}{RT}$$

where V is the reactor volume

Y_{SiH_4} is the mole fraction of silane

k_1 is the gas phase rate constant

and the silane effluent is given by:

$$Y_{SiH_4} = \frac{-(q_{in} + k_1 V) \pm [(q_{in} + k_1 V)^2 + 4(qY_{SiH_4})_{in} k_1 V]^{1/2}}{2k_1 V}$$

where q_{in} is the volumetric flow into the reactor.

A typical result of these equations is a calculation of the amount of hydrogen generated in the reactor as a function of deposition rate and the gas feed rate to each section of the reactor. These results can be summarized in the following table.

TABLE 6-2

FRACTION OF HYDROGEN GENERATED IN A SILANE DISCHARGE FOR DIFFERENT FLOW RATES AND DEPOSITION RATES

Gas Feed Rate[2] (SCCM)	Film Growth Rate[1] (Å/min) 250	600	1000
300	.10	.23	.36
600	.05	.12	.20
900	.035	.08	.14
1300	---	---	.10

[1]Area of deposition approximately 2 times grid area

[2]Gas rate to each sector of reactor

The models developed in Subcontract STF-2 are general and allow description of the effect of the gas flow distribution system design on gas composition for various deposition rates. Future system designs can thus be evaluated for uniformity of film properties throughout the reactor vessel.

The second major area of this subcontract has been in the development of heat transfer equations to determine optimum heating and cooling configurations for an in-line type reactor.

The energy balance equation to describe transient temperature profiles, where radiation is the most significant mode of heat transfers, for a single flat plate with heated surfaces on either side can be described as follows:

$$VC_p \frac{dT}{dt} = Q_{n-1,n} + Q_{n,n+1}$$

where T_n is the temperature of sheet n.

$Q_{n-1,n}$ is the heat transfer from surface n-1 to substrate n, $Q_{n,n+1}$ is the heat transfer from surface n+1 to substrate n, and ρ , V, C_p are the density, volume and heat capacity of sheet n.

This equation can easily be expanded to account for the effect of electrodes of various transparencies and thermal properties between the heated surfaces and the substrate. A further generalization to multiple substrates can also be modeled as well as the cooling rate of the substrates at the exit of the reactor vessel.

The purpose of this model is to determine optimum time-temperature relationships for heating and cooling glass substrates in in-line reactors. Substrate heaters and cooling surfaces can thus be maintained at temperatures calculated to reduce the stress on glass substrates to minimize breakage and still obtain high throughputs.

SECTION 7.0

REFERENCES

1. D.E. Carlson, A. Catalano, R.V. D'Aiello, C.R. Dickson, and R.S. Oswald, AIP Conf. Proc. No. 120 (AIP, NY, 1984) p. 234.

2. A. Delahoy and R.W. Griffith, Conf. Record of 15th IEEE Photovoltaic Specialists Conf. (IEEE, NY, 1981) p. 704.

3. Y. Tawada, K. Tsuge, M. Kondo, H. Okamoto and Y. Hamakawa, J. Appl. Phys. 53, 5273 (1982).

4. D.E. Carlson, C.W. Magee and A.R. Triano, J. Electrochem. Soc. 126, 688 (1979).

5. R.S. Crandall, Phys. Rev. B24, 7457 (1981).

6. R.S. Crandall, D.E. Carlson, A. Catalano, and H.A. Weakliem, Appl. Phys. Lett. 44, 200 (1984).

7. C.C. Tsai, J.C. Knights, R.A. Lujan, B. Wacker, B.L. Stafford and M.J. Thompson, J. Non-Cryst. Solids 59 & 60, 731 (1983).

8. B.G. Yacobi, R.J. Matson, C.R. Herrington and Y.S. Tsuo, J. Appl. Phys. 56, 3011 (1984).

9. S. Hasegawa, S. Narikawa and Y. Kurata, Philos. Mag. B48, 431 (1983).

10. J.S. Maa and S.J. Lin, Thin Solid Films 64, 63 (1979).

11. D.E. Carlson, R.W. Smith, C.W. Magee and P.J. Zanzucchi, Philos. Mag. B45, 51 (1982).

12. D.E. Carlson, J. Vac. Sci. Technol. 20, 290 (1982).

13. R.S. Crandall, D.E. Carlson, A. Catalano, H.A. Weakliem, Appl. Phys. Lett. 44, 200 (1984).

14. N. Nakamura, S. Tsuda, T. Takahama, M. Nishikuni, K. Watanobe, M. Ohnishi and Y. Kuwano, AIP Conf. Proc., No. 120 (AIP, NY, 1984) p. 303.

15. H. Sakai, A. Asano, M. Nishiura, M. Kamiyama, Y. Uchida and H. Haruki, ibid., p. 318.

16. S. Guha, Appl. Phys. Lett. 45, 569 (1984).